[American Journal of Science, Vol. 321, January-February, 2021, P. 178–205, DOI 10.2475/01.2021.05]

LATE PALEOZOIC TECTONIC TRANSITION FROM SUBDUCTION TO COLLISION IN THE CHINESE ALTAI AND TIANSHAN (CENTRAL ASIA): NEW GEOCHRONOLOGICAL CONSTRAINTS

PENGFEI LI*,**,†, MIN SUN***, CHAO YUAN*,**, FRED JOURDAN****, WANWAN HU*,**, and YINGDE JIANG*,**

ABSTRACT. The evolution of the largest accretionary orogen in the world, the Central Asian Orogenic Belt (CAOB), involved a prolonged accretion history since the Neoproterozoic, followed by a collisional phase in response to the closure of the Paleo-Asian Ocean in the latest Paleozoic. The exact process for the tectonic transition from subduction to collision is still poorly constrained. Here we address this issue by investigating the late Paleozoic tectonic evolution of the Chinese Altai and Tianshan orogens in the western CAOB. We provide new geochronological data from two areas of the Chinese Altai and Tianshan orogens, which allow us to link polyphase deformation with orogenic processes. In the Fuyun area of the Chinese Altai Orogen, we conducted monazite U-Pb dating on four samples that show pervasive foliations with the originally sub-horizontal orientation (D_{S2}/D_{Q2}). The monazite U-Pb ages cluster at ~284 to 281 Ma, which interpreted to represent the time of sub-horizontal foliations (D_{S2}/D_{Q2}) that may result from orogen-parallel extension related to the collision of the Chinese Altai Orogen with the East Junggar Terrane. Farther south, in the Gangou area of the Chinese Tianshan Orogen, we obtained a muscovite $^{40}Ar/^{39}Ar$ plateau age of 256.6 ± 0.6 Ma for a mica schist from the dextral South Central Tianshan Shear Zone. This age confirms the Permian activity of dextral strike-slip deformation (D_{CT4}) in the Chinese Tianshan Orogen. In contrast, three mylonitic schist/granitoid samples from the dextral Main Tianshan Shear Zone are characterized by $^{40}Ar/^{39}Ar$ plateau ages of 353.9 ± 1.9 Ma (biotite), 353.9 ± 1.5 Ma (biotite) and 352.1 ± 0.7 Ma (muscovite). We interpret these early Carboniferous ages to either represent a pre-Permian dextral shearing event, or to record an early Carboniferous tectono-thermal event with recrystallized micas not reset during the Permian strike-slip deformation (D_{CT4}). An additional $^{40}Ar/^{39}Ar$ plateau age of 280.9 ± 0.5 Ma (hornblende) from a mafic dike (dolerite) that crosscuts macroscopic folds (D_{ST2}) in the southern Chinese Tianshan Orogen, provides a minimum time constraint for these folds. This age supports the simultaneous folding deformation (D_{ST2}) with dextral shearing (D_{CT4}) in the Chinese Tianshan Orogen. Combined with a comprehensive synthesis of available geological and geochronological data, we argue that orogen-parallel extension and transpressional tectonics might have played a significant role in the late Paleozoic arc/continental amalgamation of the western CAOB.

Key words: Central Asian Orogenic Belt, tectonic transition, Chinese Altai, Chinese Tianshan, geochronology, shear zone

INTRODUCTION

The Central Asian Orogenic Belt (CAOB), stretching from the Ural Mountains to the Pacific margin, represents the largest accretionary orogen on Earth. The prolonged evolution of this giant orogenic collage from Neoproterozoic to late Paleozoic, involved the interaction of a large number of magmatic arcs, microcontinental blocks, and oceanic materials (Windley and others, 2007; Wilhem and others, 2012; Xiao and

* State Key Laboratory of Isotope Geochemistry, Guangzhou Institute of Geochemistry, Chinese Academy of Sciences, Guangzhou, 510640, China
** CAS Center for Excellence in Deep Earth Science, Guangzhou, 510640, China
*** Department of Earth Sciences, The University of Hong Kong, Pokfulam Road, Hong Kong, China
**** Western Australian Argon Isotope Facility, Department of Applied Geology and John de Laeter Research Centre, Curtin University, GPO Box U1987, Perth, Western Australia 6845, Australia
† Corresponding Author: Pengfei Li, pengfeili@gig.ac.cn; pengfeili2013@gmail.com

others, 2015; Şengör and others, 2018). Several generations of geologists have made an effort to understand the orogenic processes of the CAOB. Şengör and others (1993) and Şengör and Natal'in (1996) proposed that the CAOB was built by oroclinal bending and the lateral stacking of a single arc system along a series of strike-slip faults. However, subsequent studies recognized multiple Mariana-, Japan-, Cordillera- and Alaska-type arc systems within the CAOB, thus suggesting an archipelago paleogeography in the Paleozoic (Windley and others, 2007; Xiao and others, 2010a; Xiao and others, 2010b; Charvet and others, 2011). These arc systems collided together following the closure of the Paleo-Asian Ocean in the latest Paleozoic (Han and others, 2011; Xiao and others, 2015; Eizenhöfer and Zhao, 2018; Han and Zhao, 2018; Zhao and others, 2018), which significantly overprinted the earlier accretion-related records. Therefore, it is imperative to understand the collisional processes of multiple arc systems in order to reconstruct the accretionary history of the CAOB.

The CAOB in NW China is characterized by the occurrence of three Paleozoic arc systems, termed from north to south: the Chinese Altai Orogen, the West/East Junggar Terrane and the Chinese Tianshan Orogen (fig. 1). The Chinese Altai Orogen was developed via Paleozoic accretion along the Siberian margin, and collided with two intra-oceanic island arc systems of the West and East Junggar terranes along the Irtysh Shear Zone (fig. 1) (Windley and others, 2002; Laurent-Charvet and others, 2003; Glorie and others, 2012; Li and others, 2015a; Li and others, 2019). The genetic link between the West and East Junggar terranes is enigmatic given the cover of the Meso-Cenozoic Junggar Basin between them (fig. 1). Farther south, the Chinese Tianshan Orogen was subjected to Paleozoic subduction processes, followed by a collisional phase that involves the amalgamation of magmatic arcs with continental blocks (for example, the Tarim Craton) (Gao and others, 2009; Charvet and others, 2011; Han and others, 2011; Wang and others, 2011b; Xiao and others, 2013; Wang and others, 2014a; Wang and others, 2018; Biske and others, 2019; Zhong and others, 2019). The tectonic transition from subduction to collision in both Chinese Altai and Tianshan orogens has been considered to occur in the latest Paleozoic (for example, Yang and others, 2007; Charvet and others, 2011; Han and others, 2011; Wang and others, 2014a; Li and others, 2017; Han and Zhao, 2018), but the exact geodynamic processes associated with the collision are still not well constrained. A series of late Paleozoic strike-slip faults, extensional fabrics and contractional structures have been recognized in the Chinese Altai and Tianshan orogens (for example, Laurent-Charvet and others, 2003; Charvet and others, 2007; Lin and others, 2009; Wang and others, 2010a; Wang and others, 2011a; Li and others, 2015a; Broussolle and others, 2018; Jiang and others, 2019; Li and others, 2020). The precise age constraint of these structures would allow us to link the polyphase deformation with tectonic processes, thus providing a better constraint for the tectonic transition from subduction to collision in both the Chinese Altai and Tianshan orogens.

In this study, we target the Fuyun area of the southern Chinese Altai Orogen and the Gangou area of the Chinese Tianshan Orogen (fig. 1), where deformation structures have been well studied (Qu and Zhang, 1994; Laurent-Charvet and others, 2003; Charvet and others, 2007; Yang and others, 2007; Wang and others, 2010b; Li and others, 2015a; Li and others, 2016; Li and others, 2020). However, the exact time of some key structures has been poorly constrained, which limits our understanding of the tectonic transition from subduction to collision in both orogens. In this work, we present new zircon/monazite U-Pb and $^{40}Ar/^{39}Ar$ ages, which together with published geochronological data, allows us to build a time framework for the late Carboniferous to Permian deformation in the Fuyun and Gangou areas. Combined with a systematic synthesis of regional deformation, magmatism and metamorphism, we investigate the geodynamic processes associated with the collision in the Chinese

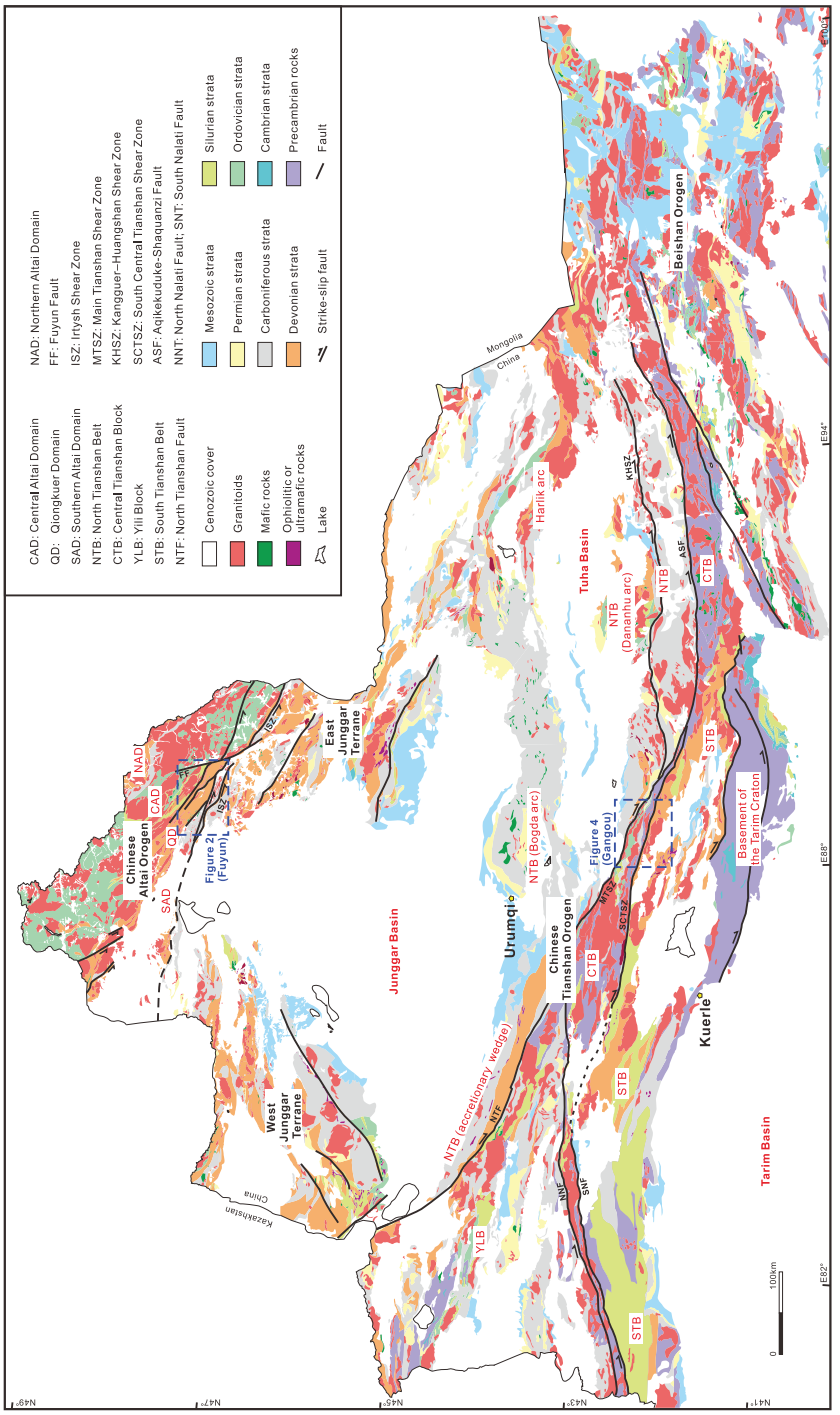

Fig. 1. Geological map of the Chinese segment of the western CAOB, which is modified from BGMRX (1993), Wang (2007) and Li and others (2017).

Altai and Tianshan orogens. Our results show that both syn-collisional extension and transpressional tectonics may have played a vital role in the late Paleozoic evolution of the Chinese Altai and Tianshan orogens.

GEOLOGICAL SETTING

The western CAOB is mainly composed of the Kazakhstan orogenic system in the southwest, and the peri-Siberian orogenic system in the northeast (for example, Xiao and others, 2015). The former is dominated by the development of island arc systems around the Kazakhstan microcontinent in the Paleozoic (Windley and others, 2007; Xiao and Santosh, 2014; Li and others, 2018). The latter is characterized by the Neoproterozoic to early Paleozoic accretion of microcontinents, island arcs and accretionary complexes along the Siberian margin, which was followed by an episode of fragmentation of the Siberian margin in the Devonian (for example, Wilhem and others, 2012; Li and others, 2019).

Chinese Altai Orogen

The Chinese Altai Orogen represents the southern segment of the peri-Siberian orogenic system (fig. 1). It can be divided into four NW-SE tectono-stratigraphic units, which are, from north to south: Northern Altai, Central Altai, Qiongkuer and Southern Altai domains (fig. 1) (Windley and others, 2002; Cai and others, 2011). The majority of the Chinese Altai Orogen is occupied by the Central Altai Domain, which mainly contains Cambrian to Silurian turbiditic and volcanic rocks of the Habahe and Kulumuti groups (Windley and others, 2002), possibly developed in an accretionary wedge in response to northeastward subduction (Xiao and others, 2009b; Long and others, 2012). This domain is separated from Devonian to Carboniferous meta-sedimentary/volcanic rocks of the Northern Altai Domain by a normal fault (Windley and others, 2002). The Qiongkuer Domain, to the south of the Central Altai Domain, comprises Devonian meta-igneous/sedimentary rocks of the Kangbutiebao and Altai formations (Windley and others, 2002), which was considered to represent a back-arc basin in response to the Devonian trench retreat (Jiang and others, 2019; Cui and others, 2020; Li and others, 2019). Farther south, the Southern Altai Domain is represented by schist, para/ortho-gneiss, amphibolite, and meta-chert of the Irtysh Complex, possibly occurring in an accretionary wedge (Briggs and others, 2007; Xiao and others, 2009a; Li and others, 2015a; Chen and others, 2019).

In the Fuyun area, Paleozoic rocks of the Southern Altai and Qiongkuer domains are well exposed (figs. 1 and 2). They were affected by multiple phases of deformation (fig. 3), likely associated with the development of the sinistral Irtysh Shear Zone during the collision of the Chinese Altai Orogen with the West/East Junggar Terrane (Qu and Zhang, 1994; Laurent-Charvet and others, 2003; Liu and others, 2013; Li and others, 2015a; Li and others, 2016; Li and others, 2017).

Chinese Tianshan Orogen

The Chinese Tianshan Orogen can be divided from north to south into the North Tianshan Belt, the Central Tianshan-Yili Block, and the South Tianshan Belt from north to south (fig. 1) (Gao and others, 1998; Xiao and others, 2004; Charvet and others, 2011; Xiao and others, 2013). Geographically, two segments of the Western and Eastern Tianshan are commonly referred to as the west and east of the Urumqi-Kuerle meridian (fig. 1).

The North Tianshan Belt in the Western Tianshan is represented by Devonian to Carboniferous volcano-sedimentary rocks and ophiolitic mélange, which has been interpreted to occur in an accretionary wedge in response to the southward subduction (Wang and others, 2006; Han and others, 2010). In contrast, a series of Paleozoic

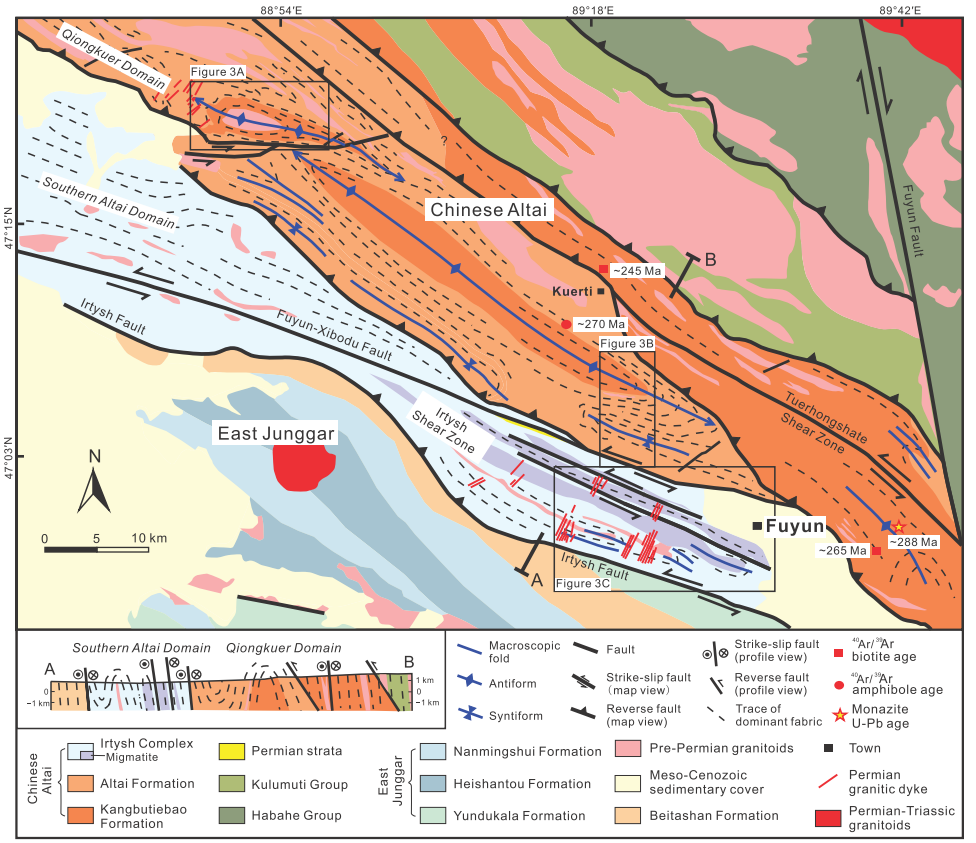

Fig. 2. Geological map of the Fuyun area in the southern Chinese Altai Orogen (after Li and others, 2017). See the location in figure 1. $^{40}Ar/^{39}Ar$ and monazite U-Pb ages are after Li and others (2015b) and Liu and others (2020).

island arcs (Bogda, Harlik, and Dananhu, fig. 1) characterize the North Tianshan Belt in the Eastern Tianshan.

Farther south, the Central Tianshan-Yili Block is separated from the North Tianshan Belt by a dextral strike-slip fault (North Tianshan Fault, or Main Tianshan Shear Zone; fig. 1) (Laurent-Charvet and others, 2003; de Jong and others, 2009; Wang and others, 2009). The triangle-shaped Yili Block comprises a Proterozoic basement that is covered by the late Paleozoic volcano-sedimentary sequence of the Yili arc (Gao and others, 1998; Zhou and others, 2001; Wang and others, 2007a; He and others, 2015; Huang and others, 2016; An and others, 2017). The Central Tianshan Block is separated from the Yili Block by the dextral North Nalati Fault (fig. 1). It is dominated by the Proterozoic basement (Huang and others, 2015 and references therein), and is covered by Ordovician to Silurian volcano-sedimentary rocks as well as Carboniferous to Permian sedimentary rocks (BGMRX, 1993; Charvet and others, 2007; Xiao and others, 2013).

The South Tianshan Belt represents the southernmost unit of the Chinese Tianshan Orogen. It consists of middle to late Paleozoic marine sedimentary-volcanic rocks as well as ophiolites, which are imbricated and stacked together along a large number of thrusts (Gao and others, 2009; Han and others, 2011; Wang and others, 2011b; Xiao and others, 2013; Jiang and others, 2014; Alexeiev and others, 2015).

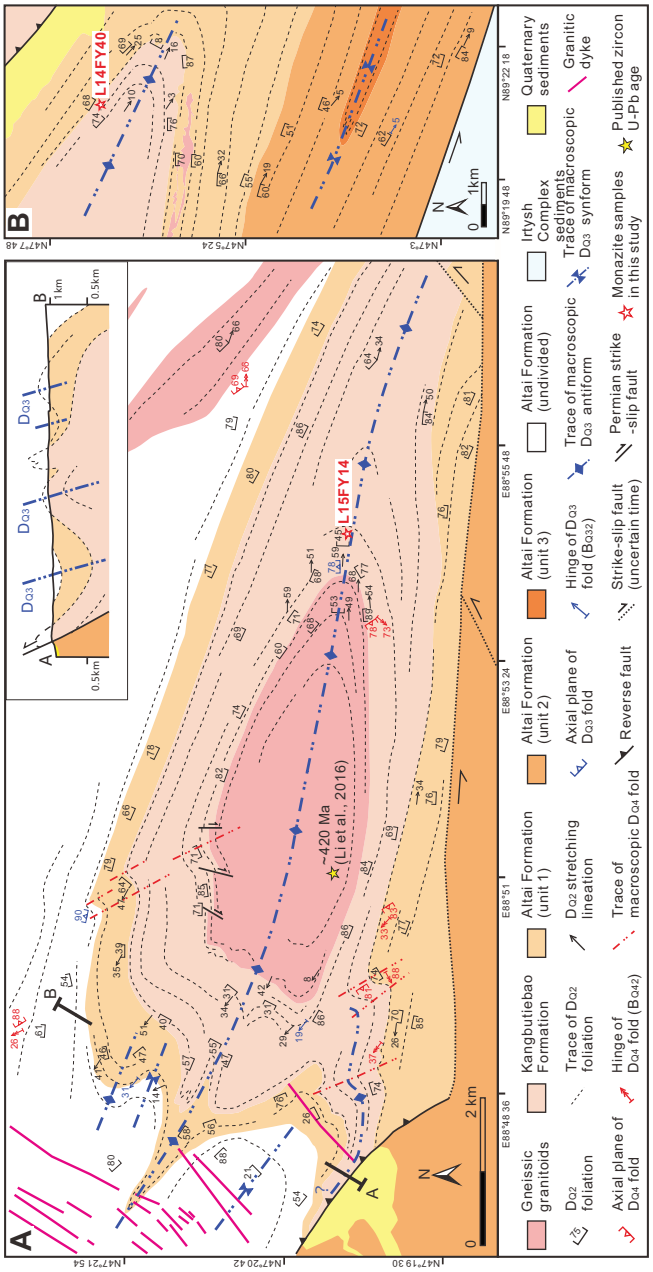

Fig. 3. (A–B) Structural map in the Qiongkuer Domain along the southern Chinese Altai Orogen (Fuyun area) (after Li and others, 2016). Note that dominant D_{Q2} foliations are folded to define ~NW-SE D_{Q3} folds and ~NNW-SSE D_{Q4} folds. The lower Altai Formation (unit 1) is characterized by quartzofeldspathic gneiss, amphibolite and banded chert, which are overlain by amphibole schist, amphibolite, and minor porphyritic meta-volcanic rocks and quartzite (unit 2) as well as gray-white quartz schist (unit 3) (Li and others, 2016). (C) Structural map in the Southern Altai Domain along the southern Chinese Altai Orogen (Fuyun area) (after Li and others, 2017). Note that D_{S2} foliations are folded to define ~NW-SE macroscopic D_{S3} folds in the southern section, but are transposed by D_{S3} axial planar foliations in the northern section. According to Li and others (2017), D_{S3} represents a phase of transpressional deformation with the development of sinistral mylonitic zones 1–4 (M1-M4) and the ~NW-SE macroscopic folds.

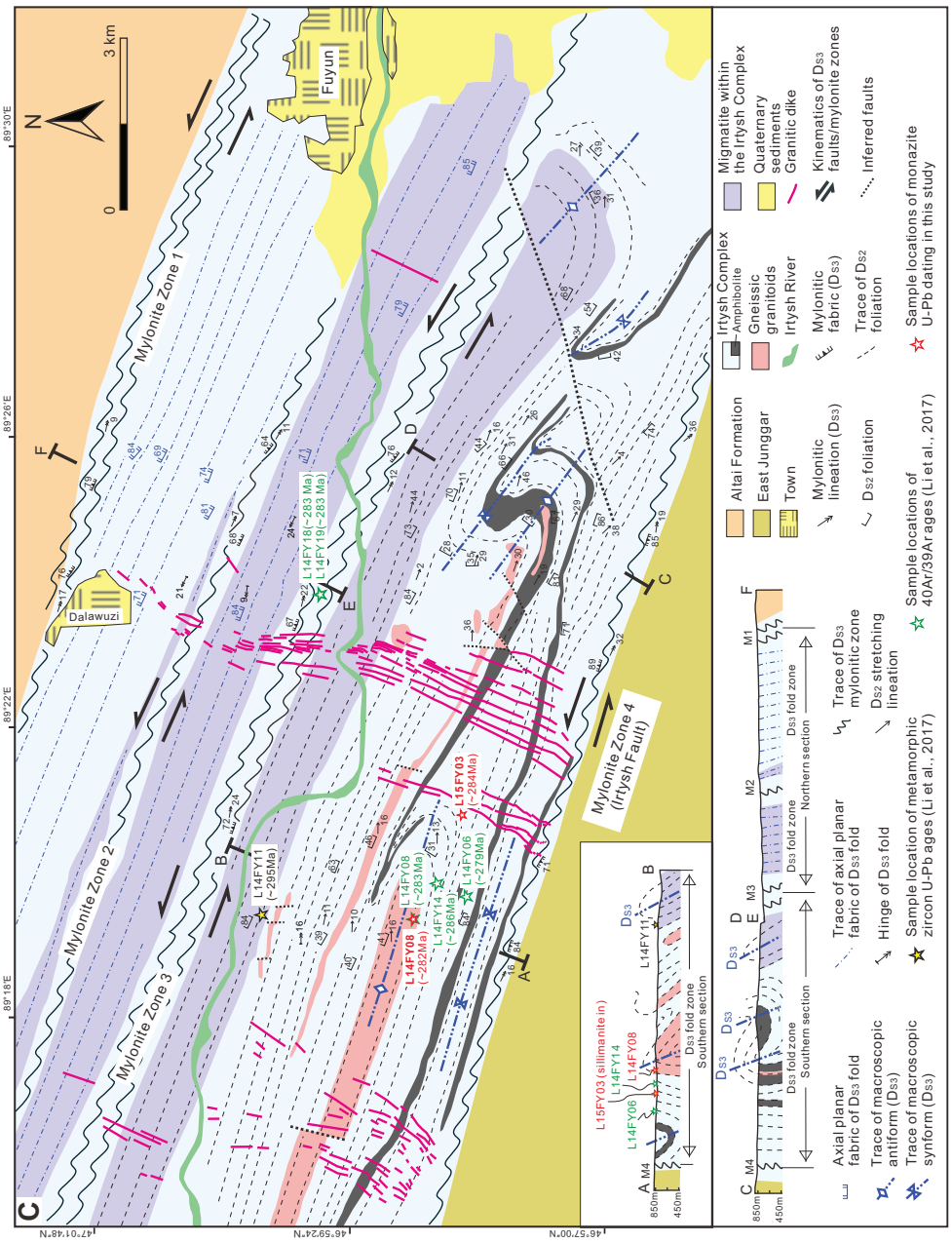

Fig. 3. Samples for $^{40}Ar/^{39}Ar$ dating by Li and others (2017) are L14FY08 (syn-D_{S2} muscovite), L14FY14 (syn-D_{S2} hornblende), L14FY06 (syn-D_{S2} biotite), L14FY18 (biotite along syn-D_{S3} shear fabric), and L14FY19 (hornblende along syn-D_{S3} shear fabric). Note that both D_{Q3} and D_{S3} folds show a similar geometry of steeply dipping axial planes and shallowly plunging hinges subparallel to ~NW-SE D_{Q2}/D_{S2} stretching lineation, which suggests an originally sub-horizontal orientation of D_{Q2}/D_{S2} foliation associated with ~NW-SE stretching lineation (subparallel to the orogenic strike) (Li and others, 2015a; Li and others, 2017).

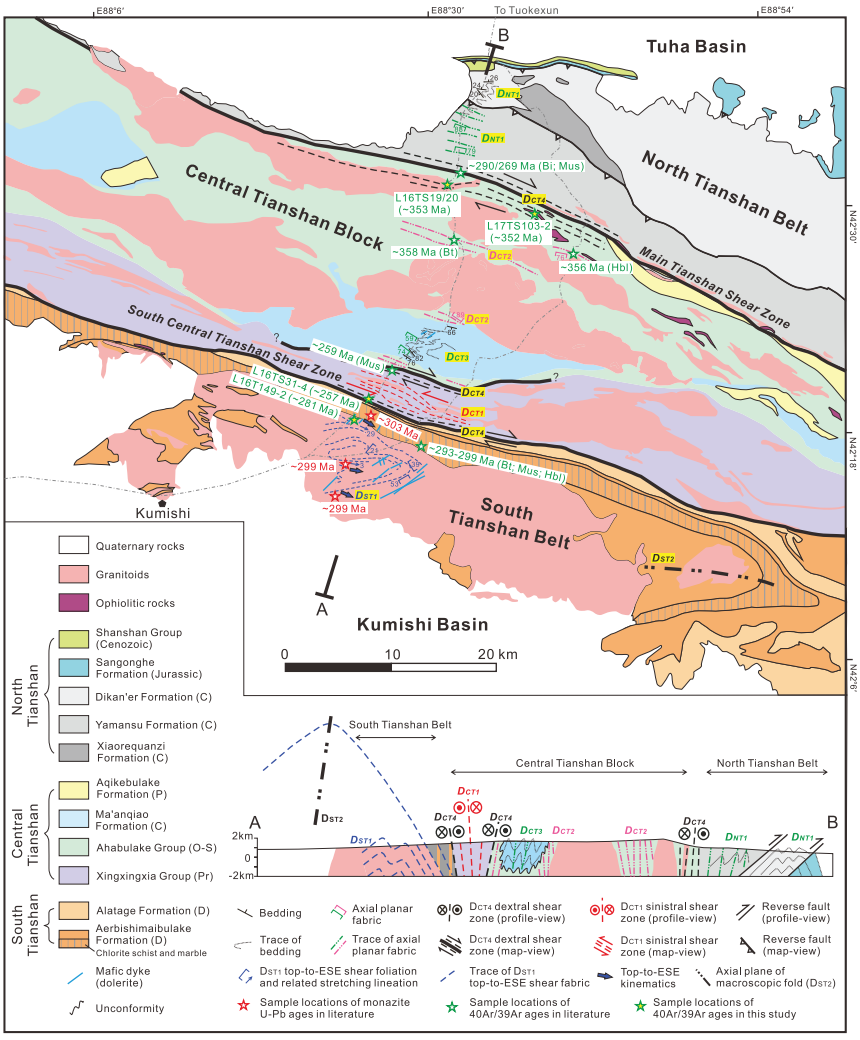

Fig. 4. Geological map of the Chinese Tianshan Orogen in the Gangou area (see the location in fig. 1; BGMRX, 1959). Structural information is mainly from Laurent-Charvet and others (2003), Deng and others (2006), Cai and others (2012b), Yang and others (2007), and Li and others (2020). According to the most recent structural synthesis by Li and others (2020), structural styles are variable across the Chinese Tianshan Orogen in the Gangou area, and are documented here. In the North Tianshan Belt, ~NW-SE folds (D_{NT1}) occur and show southward increase of shortening strain as indicated by the occurrence of axial planar foliation in the southern North Tianshan Belt. Four phases of deformation (D_{CT1}-D_{CT4}) characterize the Central Tianshan Block, with earlier sinistral strike-slip deformation (D_{CT1}) along the South Central Tianshan Shear Zone at ~399 Ma and ~NE-SW shortening at ~356 Ma as indicated by penetrative foliation in the Ahabulake Group (D_{CT2}), followed by Late Carboniferous D_{CT3} folding in the Ma'anqiao Formation and Permian dextral shearing deformation (D_{CT4}). Note that D_{CT3} axial plane cleavage is non-developed in the lower part of the Ma'anqiao Formation that unconformably overlies the strongly foliated Ahabulake Group, suggesting different generations of structures above and below the unconformity. The kinematics across the South Central Tianshan Shear Zone is variable (sinistral in the central zone, and dextral in the northern and southern zones). Farther south, ~E-W macroscopic folds (D_{ST2}) are crosscut by mafic dikes (dolerite) in the South Tianshan Belt. The earlier top-to-ESE shearing fabric (D_{ST1}) is associated with ~WNW–ESE stretching lineation subparallel to the hinge of D_{ST2} fold, which together with steeply dipping axial plane of D_{ST2} folds, indicates an originally sub-horizontal D_{ST1} foliation and ~WNW–ESE stretching lineation subparallel to the orogenic strike. For references of geochronological data, see fig. 9. Abbreviations: Permian (P), Carboniferous (C), Devonian (D), Ordovician to Silurian (O-S); Precambrian (Pr); Biotite (Bt); Muscovite (Ms); hornblende (Hbl).

TABLE 1

Summary of sample description and locations, lithological characteristics, and ages

Sample no.	Orogenic segment	Stratigraphic or tectonic units	Lithology	Location (WGS84)	Zircon U-Pb age	Monazite U-Pb age	$^{40}Ar/^{39}Ar$ age
L14FY40	Chinese Altai Orogen	Qiongkuer Domain	Leucogranite showing a penetrative D_{Q2} fabric, and comprising quartz and feldspar, as well as minor chlorite and opaque minerals.	47° 7'13"N; 89°21'12"E	409.7±1.8 Ma	281.9±1.8 Ma	
L15FY14		Qiongkuer Domain (Kangbutiebao Formation)	Mica schist with a pervasive D_{Q2} fabric and a mineral assemblage of quartz, feldspar, biotite, sillimanite, staurolite and kyanite.	47°20'14"N; 88°54'39"E		280.5±1.2 Ma	
L14FY08		Southern Altai Domain	Gneissic granitoid with a penetrative D_{S2} fabric and a major mineral assemblage of quartz, feldspar, biotite, and muscovite.	46°58'49"N; 89°19'19"E		281.7±1.7 Ma	283.0±1.2 Ma (Li and others, 2007)
L15FY03		Southern Altai Domain (Irtysh Complex)	Sillimanite biotite schist with a penetrative D_{S2} fabric and a major mineral assemblage of quartz, biotite, sillimanite, kyanite and garnet.	46°58'18"N; 89°20'41"E		284.2±1.4 Ma	
L16TS19-1 /L16TS19-2	Chinese Tianshan Orogen	Main Tianshan Shear Zone	Mylonitized granitoid with a dextral shear fabric and a major mineral assemblage of quartz, feldspar and biotite.	42°31'26"N; 88°31'46"E	428±10 Ma (Shi and others, 2007)		353.9±1.9 Ma /~352 Ma (biotite)
L16TS20		Main Tianshan Shear Zone	Mylonitized granitoid with a dextral shear fabric and a major mineral assemblage of quartz, feldspar and biotite.	42°31'26"N; 88°31'46"E	428±10 Ma (Shi and others, 2007)		353.9±1.5 Ma (biotite)
L17TS103-2		Main Tianshan Shear Zone	Mica schist showing a dextral shear fabric and containing quartz, feldspar, muscovite, and minor sillimanite and garnet.	42°29'24"N; 88°37'34"E			352.1±0.7 Ma (muscovite)
L17TS31-4		South Central Tianshan Shear Zone	Mica schist with a dextral shear fabric (D_{CT4}) and a major mineral assemblage of quartz, feldspar, muscovite and biotite.	42°19'34"N; 88°26'14"E			256.6±0.6 Ma (muscovite)
L17TS149-2		South Tianshan Belt	Mafic dike (dolerite) that crosscut ~E-W macroscopic folds (D_{ST2}) and consists of phenocrysts of hornblende, K-feldspar, pyroxene, and olivine in a groundmass of plagioclase and pyroxene	42°18'42"N; 88°24'11"E			280.9±0.5 Ma (hornblende)

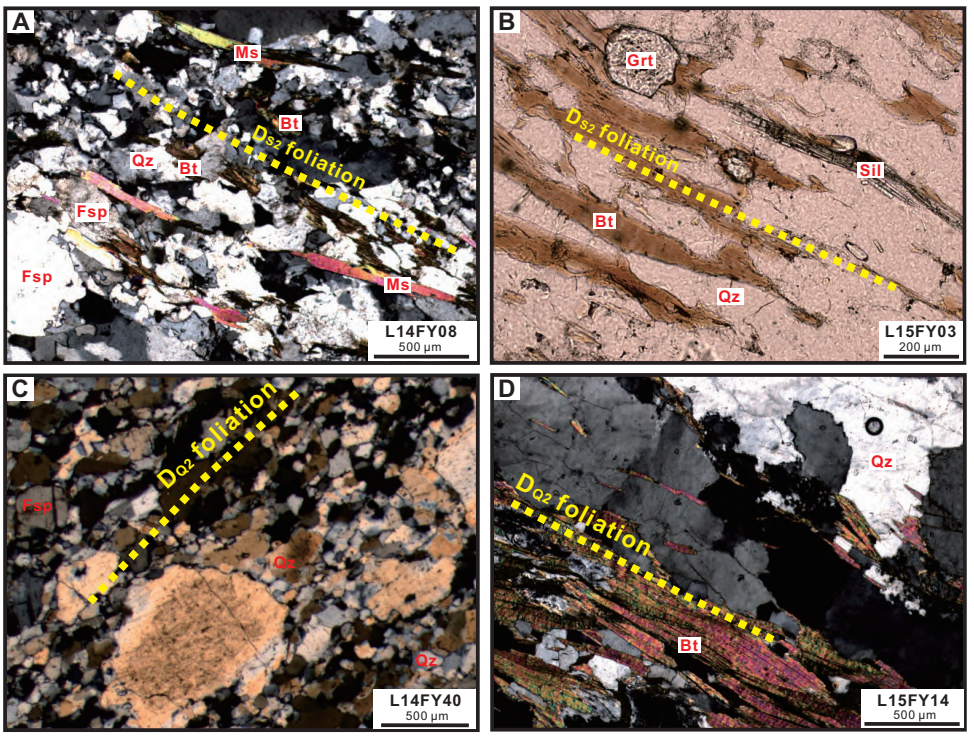

Fig. 5. Photomicrographs of samples for zircon and monazite U-Pb dating in the southern Chinese Altai Orogen (Fuyun area; see sample location in fig. 3). (A) Gneissic granitoid (sample L14FY08) from the Southern Altai Domain, with a pervasive D_{S2} fabric defined by oriented muscovite and biotite. (B) Mica schist (sample L15FY03) from the Southern Altai Domain, showing a D_{S2} foliation indicated by preferred alignment of biotite and sillimanite. (C) Shape-preferred orientation of quartz defining a D_{Q2} fabric in a leucogranite sample (L14FY40) from the Qiongkuer Domain. (D) Mica schist (sample L15FY14) from the Qiongkuer Domain, with a D_{Q2} fabric defined by preferred alignment of biotite. Mineral abbreviations: Muscovite (Ms); Biotite (Bt); Quartz (Qz); Feldspar (Fsp); Garnet (Grt).

In the Gangou area (figs. 1 and 4), the North Tianshan Belt is composed of Carboniferous andesite, volcaniclastic rocks and clastic sedimentary rocks (BGMRX, 1959), which may represent the westernmost segment of the Dananhu arc in the Eastern Tianshan (fig. 1). The North Tianshan Belt is bounded with the Central Tianshan Block by the Main Tianshan Shear Zone with a dextral strike-slip movement (Laurent-Charvet and others, 2003; Yang and others, 2009; Cai and others, 2012b; Li and others, 2020). Rocks in the Central Tianshan Block are mainly represented by Precambrian gneiss, quartzite, mica schist, amphibolite, and marble of the Xingxingxia Group, Ordovician–Silurian meta-sedimentary/volcanic rocks of the Ahabulake Group, as well as lower Carboniferous sedimentary rocks of the Ma'anqiao Formation (fig. 4) (BGMRX, 1959). A strike-slip shear zone (termed the South Central Tianshan Shear Zone; fig. 4) has been recognized along the southern margin of the Central Tianshan Block (fig. 4) (Yin and Nie, 1996; Shu and others, 1999; Laurent-Charvet and others, 2003; Charvet and others, 2007; Cai and others, 2012b). Farther south, the South Tianshan Belt, mainly comprises Early to Middle Devonian mica schist, quartz schist, and marble (fig. 4) (BGMRX, 1959). Multiple phases of deformation have affected rocks in the Gangou area (see below), and these deformation phases were considered to be associated with the amalgamation of the North Tianshan island arcs, the Central Tianshan Block

and the Tarim Craton (Laurent-Charvet and others, 2003; Yang and others, 2007; Charvet and others, 2011; Li and others, 2020).

GEOCHRONOLOGY

Sample Descriptions

Chinese Altai Orogen.—Four samples were collected in the Fuyun area along the southern Chinese Altai Orogen with an aim to constrain the deformation time (fig. 3 and table 1). Two of them (L14FY08 and L15FY03) are from the Southern Altai Domain (fig. 3C). According to Li and others (2015a, 2017), three generations of structures were recognized in this domain (D_{S1}-D_{S3}; fig. 3C). D_{S1} foliation locally occurs in low strain zones, and is strongly overprinted by D_{S2} foliation. D_{S3} represents a phase of transpressional deformation that produces the ~NW-SE macroscopic folds and a series of sinistral strike-slip mylonite zones (fig. 3C). The fact that D_{S3} folds are characterized by steeply dipping axial planes and sub-horizontal hinges parallel to ~NW-SE D_{S2} stretching lineation and the orogenic strike, suggests that the original D_{S2} foliation was sub-horizontal and the original orientation of D_{S2} stretching lineation was shallowly plunging and parallel to the orogenic strike (Li and others, 2015a). Sample L14FY08 is a gneissic granitoid from the core area of a D_{S3} antiform (fig. 3C). It mainly consists of quartz, feldspar, biotite, and muscovite, and is characterized by the occurrence of D_{S2} foliation and stretching lineation (fig. 5A). Syn-D_{S2} muscovite from this sample yielded an $^{40}Ar/^{39}Ar$ plateau age of 283±1.2 Ma (Li and others, 2017). Sample L15FY03 is a sillimanite biotite schist with a D_{S2} foliation that is associated with a stretching lineation (fig. 5B). D_{S1} foliation is not recognized in these two samples, and is considered to be completely transposed by the dominant D_{S2} foliation.

Two additional samples (L14FY40 and L15FY14) are from the Qiongkuer Domain farther north (figs. 3A and 3B). In this domain, four phases of deformation were defined (D_{Q1}-$D_{Q4;}$ figs. 3A and 3B) (Li and others, 2016). The D_{Q1} fabric locally occurs and is commonly transposed by the dominant D_{Q2} foliation (Li and others, 2016). Similarly to D_{S2} in the Southern Altai Domain, D_{Q2} foliation shows a sub-horizontal orientation before D_{Q3} folding, and is associated with ~NW-SE shallowly-plunging stretching lineation subparallel to the orogenic strike (Li and others, 2016). D_{Q2} foliations are folded to define ~NW-SE tight-close upright D_{Q3} folds and ~NNW-SSE gentle D_{Q4} folds (figs. 3A and 3B) (Li and others, 2016). Sample L14FY40 is a foliated leucogranite that comprises quartz, feldspar, as well as minor chlorite and opaque minerals. The oriented chlorite and quartz preferred orientation defines a D_{Q2} foliation (fig. 5C). Sample L15FY14 is a mica schist with a mineral assemblage of biotite, quartz, feldspar, sillimanite, staurolite and kyanite. A D_{Q2} foliation is defined by oriented biotite in this sample (fig. 5D). The earlier D_{Q1} fabric is not recognized in both samples, and is interpreted to be transposed by the dominant D_{Q2} foliation.

Chinese Tianshan Orogen.—Five samples were taken in the Gangou area of the Chinese Tianshan Orogen with the aim of constraining the timing of deformation (fig. 4 and table 1). According to Li and others (2020), the Gangou area is characterized by variable structural patterns across the whole Chinese Tianshan Orogen (fig. 4).

Carboniferous rocks were deformed to form ~NW-SE folds (D_{NT1}) in the North Tianshan Belt (fig. 4). Farther south, four generations of structures (D_{CT1}-D_{CT4}) were recognized in the Central Tianshan Block, with the earliest being sinistral shearing (D_{CT1}) along the South Central Tianshan Shear Zone at ~399 Ma, followed by ~356 Ma NE-SW contraction (D_{CT2}) that deformed the Ordovician–Silurian Ahabulake Group (fig. 4) (Li and others, 2020). Late Carboniferous to Permian deformation is characterized by ~NE-SW contraction (D_{CT3}) that folded the lower Carboniferous

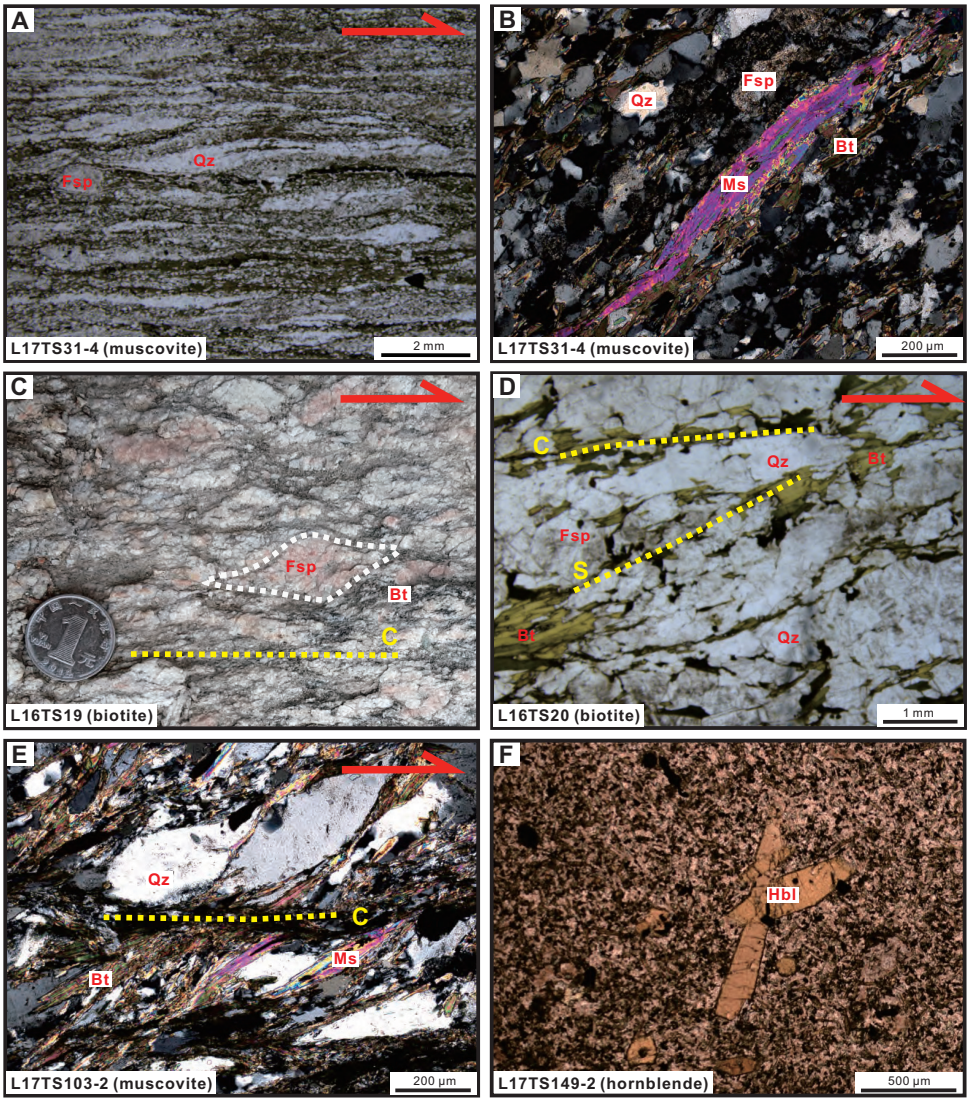

Fig. 6. Photomicrographs of samples for $^{40}Ar/^{39}Ar$ analysis in the Chinese Tianshan Orogen (Gangou area; see sample locations in fig. 4). (A–B) Mica schist sample (L17TS31-4) with dextral shear sense indicated by sigma-shaped quartz ribbon, and a mineral assemblage of quartz, feldspar, muscovite and biotite. (C–D) Mylonitic granitoids (samples L16TS19 and L16TS20) with dextral shear sense shown by sigma-shaped feldspar and S-C fabric. (E) Mica schist sample (L17TS103-2) from the Main Tianshan Shear Zone, in which S-C fabric shows dextral kinematics. (F) Dolerite sample (L17TS149-2) from mafic dike in the South Tianshan Belt, showing hornblende phenocrysts in a groundmass of plagioclase and pyroxene. Mineral abbreviations: Muscovite (Ms); Biotite (Bt); Quartz (Qz); Feldspar (Fsp); Hornblende (Hbl).

Ma'anqiao Formation, as well as dextral ductile shearing (D_{CT4}) along the northern and southern margins of the Central Tianshan Block (the Main Tianshan Shear Zone and the South Tianshan Shear Zone) (fig. 4) (Li and others, 2020). Both dextral and sinistral kinematics were reported along the South Central Tianshan Shear Zone in the Gangou area (Laurent-Charvet and others, 2003; Deng and others, 2006). Li and others (2020) recognized spatial variation in kinematics across the South Central

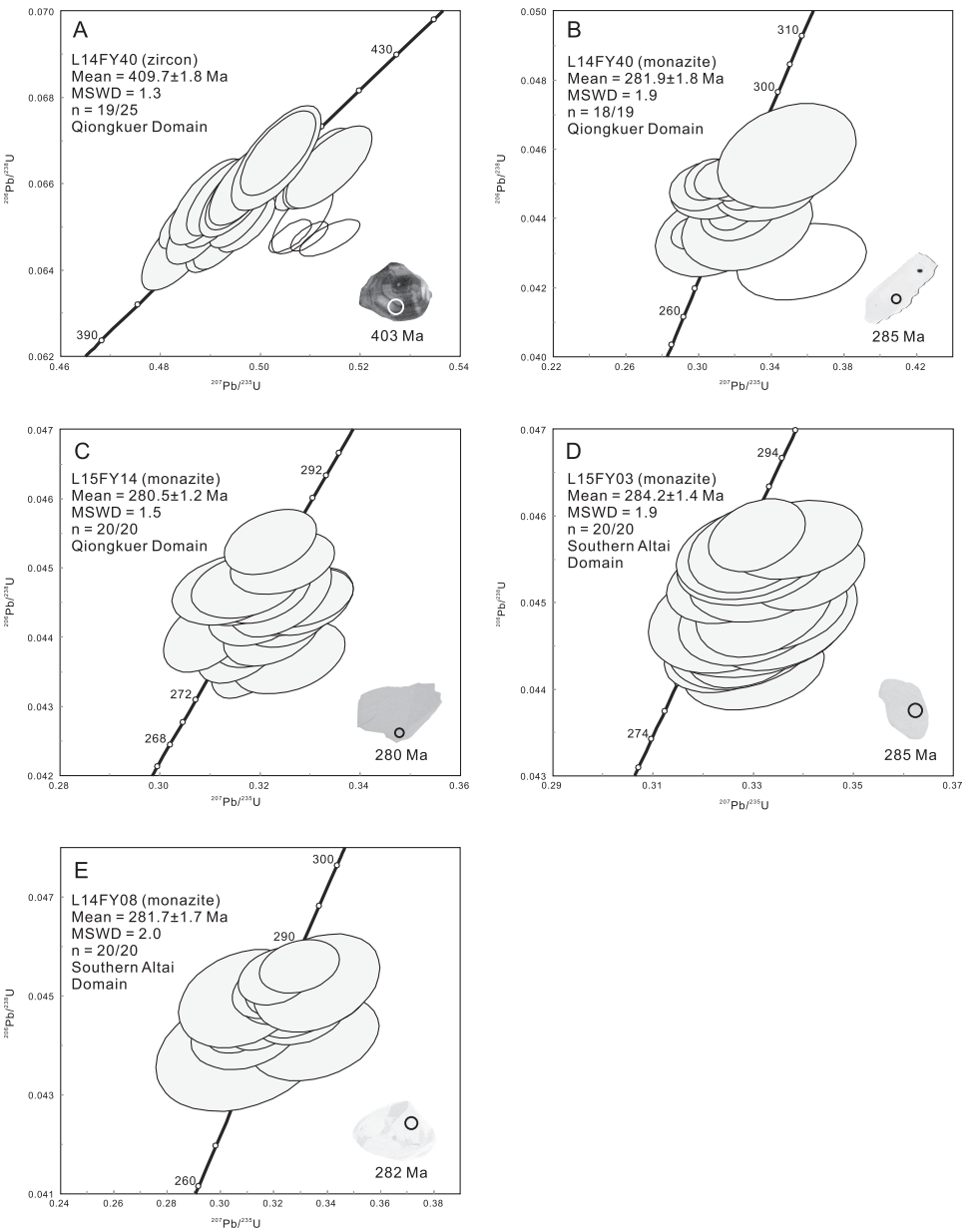

Fig. 7. Concordia diagrams for zircon U–Pb analyses. Circles with diameters of 30 μm (zircon) and 16 μm (monazite) in the CL and BSE images, indicate locations of U-Pb analyses.

Tianshan Shear Zone, with sinistral shearing (D_{CT1}) in the central zone and dextral kinematics (D_{CT4}) in the northern and southern zones (fig. 4). We collected one sample (L17TS31-4) along the southern zone of the South Central Tianshan Shear Zone (fig. 4), which is a mica schist with dextral shearing fabric (D_{CT4}; fig. 6A), that mainly consists of quartz, feldspar, muscovite and biotite (fig. 6B). In addition, three samples (L16TS19, L16TS20 and L17TS103-2) were collected along the Main Tianshan Shear

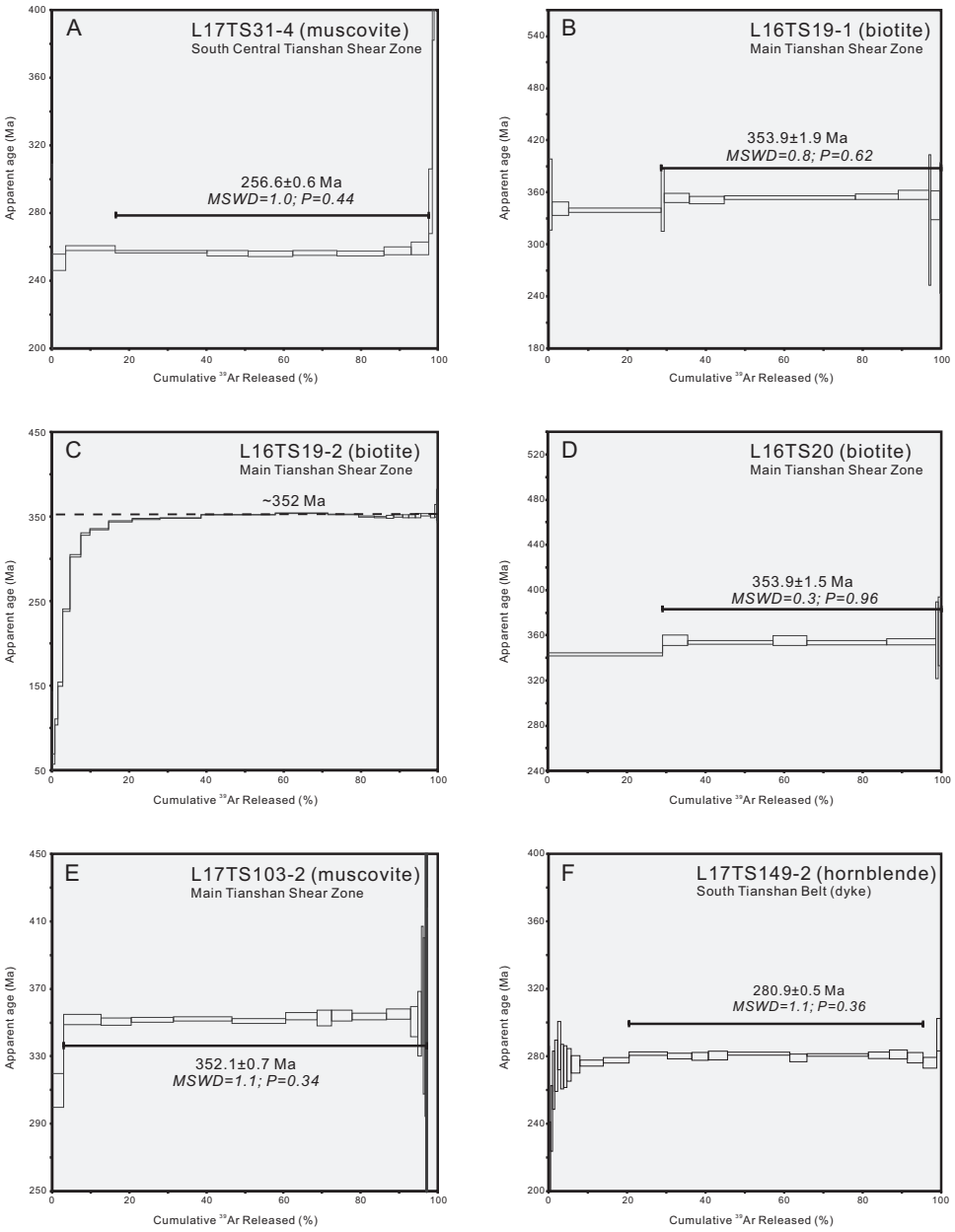

Fig. 8. $^{40}Ar/^{39}Ar$ step-heating results for analyzed samples. Note that two grains of sample L16TS19 were analyzed, and one of them gives a less reliable error age of ~352 Ma (L16TS19-2; fig. 8C).

Zone (fig. 4). Samples L16TS19 and L16TS20 are from the same mylonitic granitoid (two localities ~10 m from each other). They are characterized by similar mineral assemblages of quartz, feldspar and biotite, and are characterized by dextral mylonitic fabric (figs. 6C and 6D). Zircons from the granitic pluton of these two samples yielded a SHRIMP U-Pb age of 428±10 Ma (Shi and others, 2007). Sample L17TS103-2 is a

mica schist that shows a dextral shearing fabric, and consists of quartz, feldspar, muscovite, as well as minor sillimanite and garnet (fig. 6E).

In the South Tianshan Belt, we collected one dolerite sample (L17TS149-2) from a mafic dike in the South Tianshan Belt, which comprises phenocrysts of hornblende, K-feldspar, pyroxene, and olivine in a groundmass of plagioclase and pyroxene (fig. 6F). The dike crosscuts ~E-W macroscopic fold structures (D_{ST2}) that deformed an earlier D_{ST1} shearing fabric (top-to-ESE kinematics; fig. 4) (Li and others, 2020). D_{ST2} folds show steeply dipping axial planes and hinges shallowly plunging to the ESE (subparallel to the D_{ST1} stretching lineation and the orogenic strike), which indicates originally shallowly-dipping D_{ST1} shearing foliation and orogen-parallel stretching lineation (prior to D_{ST2} folding) (Li and others, 2020).

Analytical Methods and Results

U-Pb geochronology was used to analyze zircon grains from one sample (L14FY40), and monazite grains from four samples (L14FY40, L15FY14, L14FY08 and L15FY03). The aim was to constrain the time of D_{S2} and D_{Q2} deformation in the Chinese Altai Orogen. The $^{40}Ar/^{39}Ar$ dating technique was used to date biotite from samples L16TS19 and L16TS20, muscovite from samples L17TS31-4 and L17TS103-2, and hornblende from sample L17TS149-2. Biotite and muscovite selected from these samples are aligned along the dextral mylonitic fabric (figs. 6A–6E), and their $^{40}Ar/^{39}Ar$ age could potentially constrain the timing of shearing deformation (D_{CT4}). Hornblende is aimed to date mafic dikes in the South Tianshan Belt that crosscut D_{ST2} folds (fig. 4), thus providing a youngest age constraint for D_{ST2}. For detailed analytical methods and data processing, see appendix.

Chinese Altai Orogen.—CL and backscatter electron images of selected analyzed zircon and monazite grains, and U-Pb analytical results are presented in figure 7 and in the Appendix. Zircon grains from sample L14FY40 in the Qiongkuer Domain are euhedral and show oscillatory zoning (fig. 7A), which together with moderate to high Th/U ratios (0.36–1.20), suggest an igneous origin. 25 analyses from this sample show age scattering above the analytical uncertainty. After excluding the oldest outlier and five discordant ages, we calculated a weighted mean $^{206}Pb/^{238}U$ age of 409.7±1.8 Ma (MSWD = 1.3).

Monazite grains from four samples show homogeneous or irregular zoning (figs. 7B–7E). Most monazite ages cluster tightly on the Concordia curve, and the age variation in different zoning domains is not detected. In the Qiongkuer Domain, sample L14FY40 yields a weighted mean $^{206}Pb/^{238}U$ age at 281.9±1.8 Ma after excluding a discordant outlier (MSWD=1.9, fig. 7B). A similar weighted mean $^{206}Pb/^{238}U$ age of 280.5±1.2 Ma (MSWD=1.5) is obtained for the other sample from the Qiongkuer Domain (L15FY14, fig. 7C). Farther south in the Southern Altai Domain, we calculated two weighted mean $^{206}Pb/^{238}U$ ages of 284.2±1.4 Ma (MSWD=1.9) and 281.7±1.7 Ma (MSWD=2.0) for samples L15FY03 and L14FY08, respectively (figs. 7D and 7E).

Chinese Tianshan Orogen.—$^{40}Ar/^{39}Ar$ analytical results are presented in figure 8 and in the Appendix. One muscovite grain from sample L17TS31-4 in the southern zone of the South Central Tianshan Shear Zone yields an $^{40}Ar/^{39}Ar$ plateau age of 256.6±0.6 Ma (fig. 8A). Both muscovite and biotite grains from three samples (L16TS19, L16TS20 and L17TS103-2) of the Main Tianshan Shear Zone give $^{40}Ar/^{39}Ar$ ages clustering at ~352 Ma (figs. 8B–8E). One biotite grain from samples L16TS19 shows relatively flat age spectra and defines an $^{40}Ar/^{39}Ar$ plateau age of 353.9±1.9 Ma (fig. 8B), which is compatible with an approximate error age of ~352 Ma from the other biotite grain from this sample (fig. 8C). Similarly, sample L16TS20 yields a biotite $^{40}Ar/^{39}Ar$ plateau age of 353.9±1.5 Ma (fig. 8D), and muscovite from sample L17TS103-2 gives an $^{40}Ar/^{39}Ar$ plateau age of 352.1±0.7 Ma (fig. 8E). One

mafic dike sample (L17TS149-2) from the South Tianshan Belt is characterized by a hornblende $^{40}Ar/^{39}Ar$ plateau age of 280.9±0.5 Ma (fig. 8F).

DISCUSSION

Late Paleozoic Tectonics of the Chinese Altai Orogen

The late Paleozoic tectonics of the Chinese Altai Orogen is characterized by a transition from subduction to collision with the island arc systems of the East/West Junggar Terrane along the Irtysh Shear Zone (Zhang and others, 2012; Tong and others, 2014; Li and others, 2017; Zhang and others, 2018; Chen and others, 2019; Jiang and others, 2019; Liu and others, 2020). The tectonic transition may have occurred in the latest Carboniferous, as indicated by: (1) the distinct detrital zircon provenance for the late Carboniferous sedimentary rocks in the Chinese Altai Orogen and the northern East/West Junggar Terrane (Li and others, 2017; Hu and others, 2020), and (2) the youngest subduction-related igneous rocks in the Chinese Altai Orogen are dated at 313 ± 13 Ma (Cai and others, 2012a). Such a tectonic transition significantly affected structural patterns in the southern Chinese Altai Orogen. In the following paragraphs, we combine new geochronological data with published ages to build a temporal framework for multiple generations of structures along the southern Chinese Altai Orogen in the Fuyun area (fig. 9), based on which we further discuss the late Paleozoic tectonic evolution of the Chinese Altai Orogen.

Li and others (2015a) recognized three phases of deformation in the Southern Altai Domain (Fuyun area, figs. 2 and 3C), with D_{S1} fabric locally recognized and transposed by D_{S2} foliation. Detrital zircons from the Irtysh Complex in the Southern Altai Domain yielded the youngest age peak at ~322 Ma (Li and others, 2015a; Li and others, 2017), which provides a maximum age constraint for the timing of D_{S1}. Samples L15FY03 and L14FY08 analyzed in this study are characterized by the development of pervasive D_{S2} fabric (figs. 5A and 5B). Monazite grains from these two samples yield U-Pb ages of 284.2 ±1. 4 Ma and 281.7 ± 1.7 Ma (figs. 7D and 7E), which could represent the time of syn-D_{S2} metamorphism. Alternatively, dated monazites may be inherited from a pre-D_{S2} deformation and metamorphic event, based on which new monazite ages could denote the time of D_{S1}. Given that monazites could have crystallized during low-grade metamorphism (<440°C) (Janots and others, 2008) and syn-D_{S2} high temperature metamorphism as indicated by the growth of syn-D_{S2} sillimanite (fig. 5B), we prefer an interpretation for new monazite ages to represent the time of D_{S2}. This interpretation is supported by ~295 Ma zircon U-Pb age from syn-D_2 leucosome (Li and others, 2017), which provides the youngest constraint for D_{S1}. On a larger scale, D_{S2} foliation is folded to define macroscopic ~NW-SE D_{S3} folds with the shallowly-plunging hinges sub-parallel to ~NW-SE orogenic strike (fig. 3C) (Li and others, 2015a). D_{S3} folding is kinematically compatible with the sinistral strike-slip deformation along the Irtysh Shear Zone, which led Qu and Zhang (1994) and Li and others (2015a) to interpret D_{S3} to represent an episode of transpressional deformation (fig. 10C). $^{40}Ar/^{39}Ar$ dating of syn-shearing hornblende and biotite along the southern Chinese Altai orogen shows that D_{S3} strike-slip deformation was active from ~283 to 265 Ma (Li and others, 2017; Hu and others, 2020).

Farther north in the Qiongkuer Domain (Fuyun area, figs. 2, 3A and 3B), four generations of structures within Devonian volcano-sedimentary rocks were reported (Li and others, 2016). D_{Q1} fabric is locally recognized, and is transposed by dominant D_{Q2} foliation that is associated with a shallowly plunging stretching lineation (figs. 3A and 3B) (Li and others, 2016). Two samples (L14FY40 and L15FY14, figs. 3A and 3B) in this study are characterized by the occurrence of the pervasive D_{Q2} fabric. Zircons from the leucogranite sample (L14FY40) give a U-Pb age of 409.7±1.8 Ma (fig. 7A), which provides a maximum age constraint for D_{Q1}-D_{Q2}. Monazite grains from this

sample yield a U-Pb age of 281.9±1.8 Ma (fig. 7B), which is younger than the ~410 Ma zircon U-Pb age (fig. 7A), but is compatible with the 280.5±1.2 Ma monazite age from the other mica schist sample (L15FY14, fig. 7C). Given the penetrative occurrence of D_{Q2} fabric in the Qiongkuer Domain and syn-D_{Q2} metamorphism up to amphibolite facies in the area of analyzed samples (Li and others, 2016), we interpret these monazite ages to represent the timing of D_{Q2}, which is compatible with the timing of D_{S2} in the Southern Altai Domain that shows a similar structural geometry as D_{Q2} (see more discussions about the structural correlation in the next paragraph). The subsequent deformation involved the occurrence of ~NW-SE D_{Q3} macroscopic folds and ~NNW-SSE D_{Q4} folds (figs. 3A and 3B). The time of these two folding events is considered to be prior to the intrusion of the ~NE-SW granitic dikes that are not affected by D_{Q3} and D_{Q4} (fig. 3A) (Li and others, 2016). Actually, ~NE-SW granitic dikes are widespread in the Fuyun area (fig. 3), and the youngest reported U-Pb zircon age of 252±2.2 Ma (Zhang and others, 2012), may provide a minimum age constraint for D_{Q3} and D_{Q4}.

New and published geochronological data together with available structural work allows for a deformation correlation across the Southern and Qiongkuer domains. Given the similar geometry and deformation time, Li and others (2016) proposed a correlation of ~NW-SE D_{S3} and D_{Q3} folds, and interpreted them together with coeval sinistral strike-slip deformation to represent a phase of transpressional deformation in the early to late Permian (figs. 9 and 10C). However, the correlation of pre-D_{S3}/D_{Q3} structures was hindered because of limited age constraints on deformation. Actually, both D_{S2} and D_{Q2} foliations are folded to define ~NW-SE macroscopic D_{S3}/D_{Q3} folds with shallowly plunging hinges subparallel to ~NW-SE D_{S2} and D_{Q2} stretching lineations (figs. 3A–3C), which suggests an originally sub-horizontal occurrence of D_{S2} and D_{Q2} foliations associated with shallowly plunging stretching lineations parallel to the ~NW-SE orogenic strike (Li and others, 2015a; Li and others, 2016). New monazite ages confirm that both D_{S2} and D_{Q2} were developed at a similar period, supporting a correlation of D_{S2} and D_{Q2} across the Qiongkuer and Southern Altai domains. The ~284 to 281 Ma monazite ages from both the Qiongkuer and Southern Altai domains are older than the syn-D_{Q2} hornblende $^{40}Ar/^{39}Ar$ age of 270.1±3.1 Ma in the Qiongkuer Domain (fig. 2) (Li and others, 2015b), but overlap within errors with syn-D_{S2} hornblende (286.7±1.2 Ma), muscovite (283.0±1.2 Ma) and biotite (279.8±1.6 Ma) (figs. 3C and 9) (Li and others, 2017) in the Southern Altai Domain. These $^{40}Ar/^{39}Ar$ ages were interpreted to represent the cooling time of analyzed syn-D_{S2}/D_{Q2} minerals through their closure temperature, which may have been linked with the regional uplift during D_{S3}/D_{Q3} transpressional deformation (Li and others, 2015b; Li and others, 2017). If this interpretation is correct, a fast transition from D_{S2}/D_{Q2} to D_{S3}/D_{Q3} can be inferred given the overlapping of monazite and $^{40}Ar/^{39}Ar$ ages, within errors. We emphasize, however, that the exact transitional time of these two deformation events is uncertain given the limited resolution of analytical methods, but could be around ~283 Ma (the mean of overlapping $^{40}Ar/^{39}Ar$ and monazite ages, fig. 9).

The development of D_{S2}/D_{Q2} sub-horizontal foliation and related orogen-parallel stretching lineation, which indicates a sub-vertical flattening and orogen-parallel stretching strain, has been attributed to the orogen-parallel extensional collapse in the Southern Altai Domain (fig. 10B) (Li and others, 2015a). Our new monazite ages (~284–281 Ma), together with previous structural work (Li and others, 2016), confirm that such an event also affected the Qiongkuer Domain in the Permian. A ~295 Ma metamorphic zircon age from syn-D_{S2} leucosome in the Southern Altai Domain could represent the time of the initial extension (Li and others, 2017). Such an age constraint (~295–283 Ma) for D_{S2}/D_{Q2} overlaps in time with ~299 to 277 Ma high

temperature metamorphism (Li and others, 2014; Wang and others, 2014b; Liu and others, 2020) and 280±10 Ma age peak of granitic magmatism (Tong and others, 2014; Tang and others, 2017) in the southern Chinese Altai Orogen. Therefore, we consider that the orogen-parallel extension (D_{S2}/D_{Q2}) may have been responsible for the high thermal gradient and the development of widespread magmatism along the southern Chinese Altai Orogen in the Permian (figs. 9 and 10B). According to Li and others (2015a), this extensional episode may have occurred post to an orogen-thickening event (D_{S1} and D_{Q1}) associated with the initial collision of the Chinese Altai Orogen with the East Junggar Terrane (fig. 10A), and was followed by a transpressional event (D_{S3}/D_{Q3} folding and sinistral shearing) related to the oblique convergence of the Chinese Altai Orogen with the East Junggar Terrane (fig. 10C). Li and others (2016) suggested that earlier transpressional deformation was characterized by a high degree of strain partioning, as indicated by the parallelism of D_{S3}/D_{Q3} fold axial planes with sinistral mylonitic zones, and strain partitioning was likely less efficient in the later stage, with a fraction of transcurrent components partitioned into ~NNW-SSE D_{Q4} folds (fig. 3A).

Late Paleozoic Tectonics of the Chinese Tianshan Orogen

The Chinese Tianshan Orogen evolved into a collisional phase in the latest Paleozoic after the closure of the southern branch of the Paleo-Asian Ocean (for example, Han and others, 2011; Xiao and others, 2013; Han and Zhao, 2018). In the Gangou area (fig. 1), such a collisional event involved the amalgamation of the Central Tianshan Block with the North Tianshan island arc system and the Tarim Craton (fig. 1). The island arc system (for example, Bogda and Dananhu arc, fig. 1) in the North Tianshan Belt likely collided with the Central Tianshan Block in the latest Carboniferous given that early Permian sedimentary rocks from the North Tianshan Belt in the Eastern Tianshan received abundant Precambrian detrital zircons sourced from the Central Tianshan Block (Zhang and others, 2016), and ~305 to 301 Ma mafic igneous rocks were characterized by the significant input of asthenospheric mantle that was likely induced by slab breakoff (Zhang and others, 2020). Farther south, the exact collisional time between the Central Tianshan Block and the Tarim Craton remains controversial, but is possibly diachronous within the period of late Carboniferous to the earliest Triassic (for example, Han and others, 2011; Xiao and others, 2013; Han and Zhao, 2018). These collisional events were accompanied by dextral shearing as well as folding along the Chinese Tianshan Orogen (fig. 1) (Shu and others, 1999; Laurent-Charvet and others, 2002; Laurent-Charvet and others, 2003; Wang and others, 2008; Wang and others, 2010a; Zhu and others, 2018; Li and others, 2020). According to Li and others (2020), deformation patterns in the Gangou area are variable across the Chinese Tianshan Orogen. Our $^{40}Ar/^{39}Ar$ ages provide new timing constraints for deformation in the Central Tianshan Block and the South Tianshan Belt as documented in the following paragraphs.

Four phases of deformation were recognized in the Gangou area of the Central Tianshan Block (D_{CT1}-D_{CT4}), with earlier subduction-related D_{CT1} sinistral shearing (~399 Ma) and D_{CT2} NE-SW contraction (~356 Ma), followed by late Carboniferous to Permian D_{CT3} NE-SW shortening deformation and D_{CT4} dextral shearing (figs. 4 and 9) (Li and others, 2020). Spatially, D_{CT1} sinistral shearing occurs in the central zone of the South Central Tianshan Shear Zone, which is bounded by two dextral mylonite zones (D_{CT4}) in the northern and southern parts of the South Central Tianshan Shear Zone (fig. 4). Muscovite separated along the syn-D_{CT4} shear fabric in the southern part of the South Tianshan Shear Zone (sample L17TS31-4, fig. 4) yields an $^{40}Ar/^{39}Ar$ age of 256.6 ± 0.6 Ma (fig. 8A), suggesting that the dextral shearing was active during this period. Actually, this phase of dextral shearing in the Permian has been widely recognized along the whole Chinese Tianshan Orogen via dating syn-

shearing minerals/intrusions (figs. 1 and 9) (Shu and others, 1999; Laurent-Charvet and others, 2003; Wang and others, 2007b; Wang and others, 2009; Cai and others, 2012b; Konopelko and others, 2013; Han and Zhao, 2018 and references therein; Li and others, 2020). In contrast, micas separated along dextral shear fabric of the Main Tianshan Shear Zone (fig. 4) yield indistinguishable pre-Permian $^{40}Ar/^{39}Ar$ plateau ages of 353.9 ± 1.9 Ma (biotite), 353.9 ± 1.5 Ma (biotite) and 352.1 ± 0.7 Ma (muscovite) (fig. 8). These new ages are older than most published $^{40}Ar/^{39}Ar$ ages along the dextral Main Tianshan Shear Zone, such as ~269 Ma muscovite $^{40}Ar/^{39}Ar$ plateau age (Laurent-Charvet and others, 2003), ~244 Ma biotite $^{40}Ar/^{39}Ar$ isochron age (Laurent-Charvet and others, 2003), ~266 Ma muscovite and biotite $^{40}Ar/^{39}Ar$ plateau ages (Yang and others, 2009), as well as ~290 Ma biotite $^{40}Ar/^{39}Ar$ plateau age (Cai and others, 2012b). A 367.6 ± 3.2 Ma $^{40}Ar/^{39}Ar$ age, which is slightly older than our $^{40}Ar/^{39}Ar$ ages, was reported for syn-shearing muscovite along the Main Tianshan Shear Zone and was interpreted to represent a phase of dextral shearing prior to the Permian (Cai and others, 2012b). Such an interpretation is supported by available quartz c-axis fabric data from the Main Tianshan Shear Zone, which give a large shearing temperature range from >650°C to <350°C (Laurent-Charvet and others, 2003; Cai and others, 2012b), thus suggesting multiple episodes of dextral shearing. Alternatively, analyzed minerals with pre-Permian $^{40}Ar/^{39}Ar$ ages may be inherited from an Early Carboniferous tectono-thermal event, and the Permian strike-slip deformation may not reset the K-Ar isotopic system of dated minerals. Indeed, inherited pre-Permian $^{40}Ar/^{39}Ar$ age components have also been reported in the dextral Talas–Ferghana strike-slip fault zone of the Kyrgyz Tianshan farther west (Rolland and others, 2013; Konopelko and others, 2017).

In the South Tianshan Belt (Gangou area), ~E-W D_{ST2} folds with shallowly plunging hinges affected the D_{ST1} fabric, and are crosscut by a series of mafic dikes (fig. 4). New $^{40}Ar/^{39}Ar$ age of hornblende (L17TS149-2) constrains the intrusion of these dikes at ~281 Ma (fig. 8F), providing a minimum timing constraint for D_{ST2}. The earlier D_{ST1} fabric was dated at ~303 to 293 Ma (Li and others, 2020), which together with new $^{40}Ar/^{39}Ar$ hornblende age constrains D_{ST2} at ~293 to 281 Ma, overlapping in time with dextral shearing along the Main Tianshan and South Central Tianshan shear zones (D_{CT4}; fig. 9). The angular relationship of ~E-W D_{ST2} folds with dextral D_{CT4} shear zones, indicates partitioning of shear strain into fold domains and discrete shear zones (fig. 10F). On a larger scale, the dextral Main Tianshan and South Central Tianshan shear zones extend into the East Tianshan (fig. 1), where positive flower structures suggest transpressional strike-slip deformation for D_{CT4} in the Permian (Shu and others, 1999; Wang and others, 2008).

New and published ages along dextral shear zones in the Chinese Tianshan Orogen demonstrate relatively right-lateral movement of the North Tianshan Belt, the Central Tianshan Block and the South Tianshan Belt along the orogenic strike in the Permian. In the Gangou area, such a lateral migration occurred post an orogen-perpendicular contractional event, as indicated by NW-SE folds in the North Tianshan Belt (D_{NT1}) and in the Central Tianshan Block (D_{CT3}) that affected Carboniferous rocks and likely resulted from the initial collisional orogeny in the Chinese Tianshan Orogen (figs. 4 and 10D) (Charvet and others, 2007; Li and others, 2020). If this tectonic interpretation is correct, a transition of convergent orientation from orthogonal to oblique may characterize the late Paleozoic collisional orogeny in the Chinese Tianshan Orogen (Gangou area). Additionally, Li and others (2020) mapped a top-to-ESE D_{ST1} shear fabric in the South Tianshan Belt (fig. 4), which was originally shallowly dipping (associated with orogen-parallel stretching lineation) prior to D_{ST2} folding and was interpreted to represent an episode of orogen-parallel extension (fig. 10E). Such an extensional episode was constrained to ~303 to 293 Ma

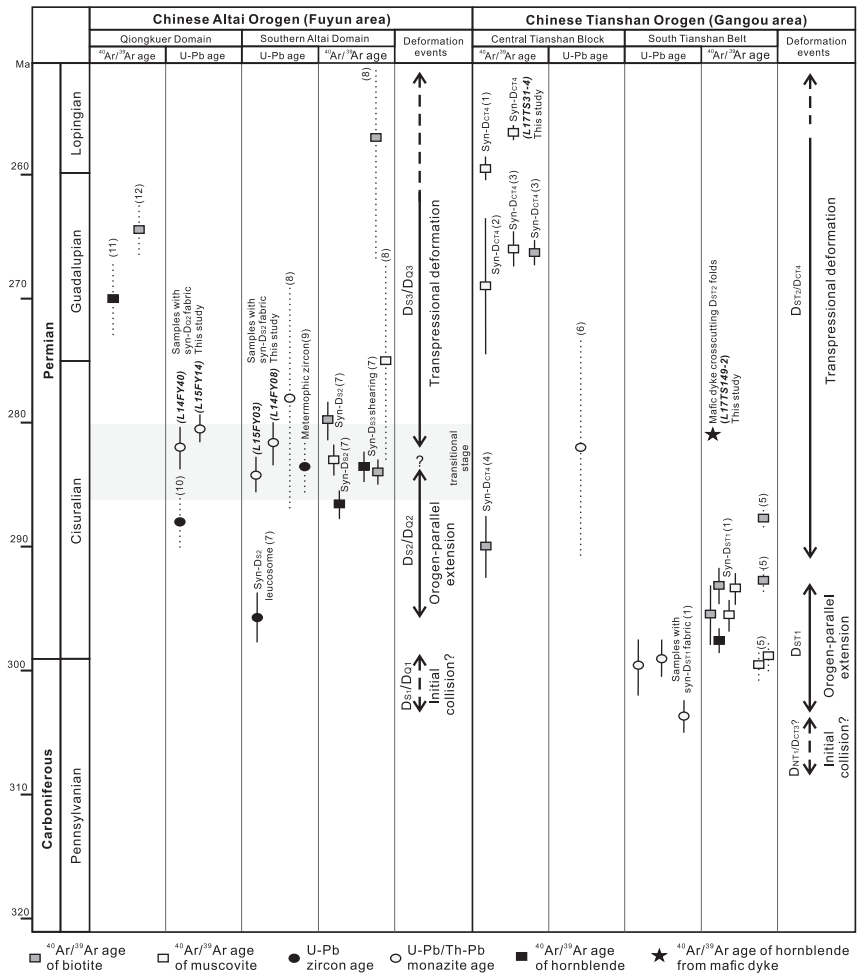

Fig. 9. A summary of late Carboniferous to Permian zircon/monazite U-Pb ages and $^{40}Ar/^{39}Ar$ plateau ages in the southern Chinese Altai Orogen (Fuyun area) and the Chinese Tianshan Orogen (Gangou area). Both areas are characterized by three late Carboniferous to Permian deformation episodes, which are interpreted to represent three stages of collisional orogeny with the initial collision followed by orogen-parallel extension and transpressional deformation (fig. 10). In the Fuyun area, the timing of deformation associated with the initial collision (D_{S1}/D_{Q1}) is constrained by the youngest detrital zircon age peak (~322 Ma) of deformed rocks (Li and others, 2015a; Li and others, 2017), while the timing of D_{S2}/D_{Q2} fabric related to syn-collisonal extension is constrained by U-Pb ages of zircons/monazites that are interpreted to be formed during the deformation (see the discussion in the text). The subsequent transpressional deformation (D_{S3}/D_{Q3}) associated with regional uplift can be constrained by $^{40}Ar/^{39}Ar$ ages. We emphasize, however, that the exact transitional time of the syn-collisonal extension with the transpressional deformation is uncertain given the limited resolution of analytical methods, but could be around ~283 Ma (the center of overlapping $^{40}Ar/^{39}Ar$ and monazite ages; the gray zone in fig. 9). In the Gangou area, structural styles are variable across the Chinese Tianshan Orogen (fig. 4). The initial collision is likely recorded by NW-SE folds in the North Tianshan Belt (D_{NT1}) and in the Central Tianshan Block (D_{CT3}) that affected Carboniferous rocks. The syn-collisional extension, which is represented by top-to-ESE D_{ST1} shear fabric in the South Tianshan Belt, is dated by syn-deformational minerals (monazite U-Pb and biotite/muscovite/hornblende $^{40}Ar/^{39}Ar$ ages). The later stage of transpressional deformation (D_{ST2}/D_{CT4}) is mainly constrained by $^{40}Ar/^{39}Ar$ ages of syn-shearing minerals. Note that dotted lines of age error in this diagram show analyzed minerals with uncertain structural context, whereas scattered $^{40}Ar/^{39}Ar$ ages or those data with hump-shaped or progressively up-stepping age spectra in the literature are not compiled. Data source: (1) Li and others (2020); (2) Laurent-Charvet and others (2003); (3) Yang and others (2009); (4) Cai and others (2012b); (5) Yang and others (2007); (6) Li and others (2008); (7) Li and others (2017); (8) Briggs and others (2007); (9) Chen others (2019); (10) Liu and others (2020); (11) Li and others (2015b).

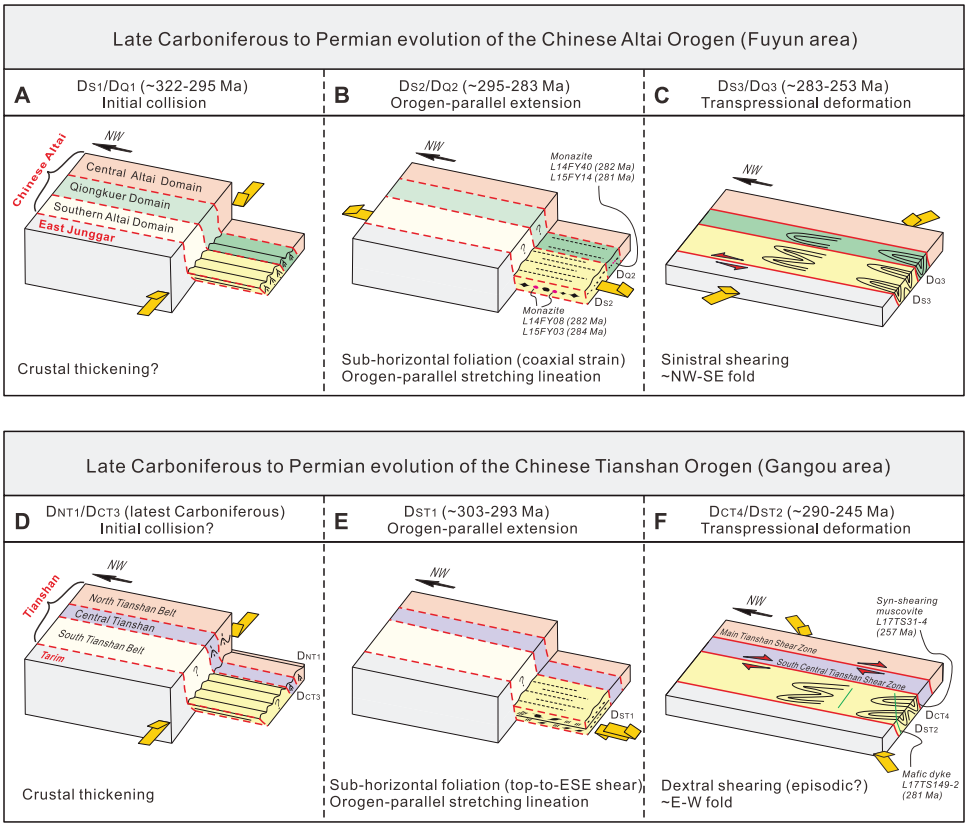

Fig. 10. (A–C) Schematic cartoons showing three stages of collision of the Chinese Altai Orogen with the East Junggar Terrane in the late Paleozoic, which was characterized by initial crustal thickening (D_{Q1}/D_{S1}), followed by the orogen-parallel extension (D_{Q2}/D_{S2}) and transpressional deformation (D_{Q3}/D_{S3}) (Li and others, 2015a). The orogen-parallel extension (fig. 10B) is inferred based on the sub-horizontal foliation and the orogen-parallel stretching lineation (D_{Q2}/D_{S2}), and the time of this event is constrained by new monazite U-Pb ages. The subsequent transpressional deformation (fig. 10C) is partitioned into folding (D_{Q3}/D_{S3}) and sinistral shearing deformation. (D–F) Schematic cartoons illustrating late Paleozoic tectonic evolution in the Chinese Tianshan Orogen (Gangou area), in which orogen-parallel extension and transpressional tectonics played a crucial role. Note that the orogen-parallel extension is indicated by top-to-ESE D_{ST1} shear fabric in the South Tianshan Belt (fig. 10E). The subsequent transpressional tectonics contributed to both folding (D_{ST2}) and dextral shearing (D_{CT4}) (fig. 10F). New hornblende $^{40}Ar/^{39}Ar$ age from a mafic sample (L17TS149-2) provides the youngest time constraint for D_{ST2} folding. Multiple episodes of dextral shearing may have occurred along the Chinese Tianshan Orogen, and the new muscovite $^{40}Ar/^{39}Ar$ age (L17TS31-4) could constrain a later phase of dextral shearing.

(fig. 9) (Li and others, 2020), which post-dates the initial collisional orogeny in the late Carboniferous, but predates the Permian strike-slip deformation in the Chinese Tianshan Orogen (fig. 10F).

Late Paleozoic Arc/Continental Amalgamation of the Western CAOB

The western CAOB is characterized by a collisional phase in the latest Paleozoic following the closure of the Paleo-Asian Ocean (Windley and others, 2007; Wilhem and others, 2012). In the north, the Chinese Altai Orogen, which represents the active margin of the Siberian Craton in the late Paleozoic (Windley and others, 2002; Li and others, 2019), collided with the East/West Junggar island arc system in the latest Carboniferous (for example, Li and others, 2017). In the south, the Chinese

Tianshan Orogen was amalgamated with the Tarim Craton and the East/West Junggar island arc system at a similar period of Late Carboniferous to Permian (Han and others, 2011; Xiao and others, 2013; Han and Zhao, 2018). Another collisional event between the Baltic Craton and the CAOB in the west was initiated in the earliest late Carboniferous (Filippova and others, 2001; Windley and others, 2007). The convergence of the Siberian, Tarim and Baltic cratons was accompanied by the development of large-scale shear zones with both dextral and sinistral kinematics in the western CAOB (fig. 1). Such a phase of strike-slip deformation could either result from oblique plate convergence (for example, Alpine Fault in New Zealand; (Norris and Toy, 2014), or accommodate the lateral migration of orogenic materials (for example, Cenozoic strike-slip faults in SE Asia) (Tapponnier and others, 1982). In the case of the western CAOB, new and published geochronological data show that the sinistral strike-slip deformation along the southern Chinese Altai Orogen and the dextral shearing in the Chinese Tianshan Orogen were both active in the Permian (Laurent-Charvet and others, 2003; Buslov and others, 2004; Wang and others, 2008; Yang and others, 2009; Cai and others, 2012b; Li and others, 2017), which illustrates the eastward escape of the East/West Junggar Terrane (fig. 1) (Wang and others, 2008; Li and others, 2015a).

An episode of orogen-parallel extensional deformation was recognized in both the Chinese Altai and Tianshan orogens (figs. 10B and 10E), following the initial arc/continental collision as documented above. Such orogen-parallel extensional structures have also been recognized in the Eastern Alps and the Himalayan Orogen, where the extensional deformation may have been linked with the gravitational potential energy of the overthickening crust (for example, Frisch and others, 2000; Selverstone, 2005; Xu and others, 2013). Such a mechanism may also be responsible for the syn-collisional extension during the late Paleozoic arc/continental amalgamation in the western CAOB (Li and others, 2015a). Importantly, the extensional deformation in the Chinese Altai and Tianshan orogens overlaps in time with regional peak magmatism and high temperature metamorphism (for example, Li and Zhang, 2004; Li and others, 2014; Tang and others, 2017; Liu and others, 2020), indicating that the syn-collisional extension may have driven orogenic thermal evolution during the late Paleozoic amalgamation of multiple arcs or continental blocks in the western CAOB.

CONCLUSIONS

(1) New monazite U-Pb ages demonstrate that the orogen-parallel extension along the southern Chinese Altai Orogen may have developed as late as ~284 to 281 Ma, which was immediately followed by an episode of transpressional deformation. The extensional deformation is likely responsible for the high thermal gradient in the early Permian as indicated by high temperature metamorphism and widespread magmatism along the southern Chinese Altai Orogen.

(2) New $^{40}Ar/^{39}Ar$ ages confirm that the Chinese Tianshan Orogen is characterized by large-scale dextral strike-slip deformation in the Permian. The occurrence of early Carboniferous $^{40}Ar/^{39}Ar$ ages along the dextral Main Tianshan Shear Zone could either represent a pre-Permian activity of dextral shearing, or result from an early Carboniferous tectono-thermal event with recrystallized micas not reset during the Permian strike-slip deformation. An additional 280.9±0.5 Ma hornblende $^{40}Ar/^{39}Ar$ age from a mafic dike that crosscuts ~E-W macroscopic folds in the southern Chinese Tianshan Orogen, provides the youngest time constraint for these folds, thus supporting the simultaneous folding deformation with dextral shearing in the Chinese Tianshan Orogen.

(3) A synthesis of available geochronological and structural data in the Chinese Altai and Tianshan orogens indicates that both syn-collisional extension and transpressional tectonics played a significant role in the structural and thermal evolution in the late Paleozoic arc/continental amalgamation of the western CAOB.

ACKNOWLEDGMENTS

This paper is dedicated to the late Prof. Dr. Alfred Kroner. Our work on the CAOB tectonics benefits from numerous discussions with Alfred. We appreciate his great help for building international collaborations in Central Asia. The paper benefits from constructive comments by Yamirka Rojas-Agramonte (Guest Editor), Bo Wang, and an anonymous reviewer. This study was financially supported by the NSF China (41872222), the National Key R&D Program of China (2017YFC0601205), the international partnership program of the Chinese Academy of Sciences (132744KYSB20200001 and 132744KYSB20190039) and Hong Kong Research Grant Council (HKU 17302317). Pengfei Li is supported by a project from Guangdong Province (2019QN01H101). This is a contribution of GIGCAS (No. IS-2962), IGCP 662 and the Chemical Geodynamics Joint Laboratory between HKU and GIGCAS.

APPENDIX

Zircon and monazite U-Pb analyses as well as $^{40}Ar/^{39}Ar$ step heating data. The analytical methods are presented in this file.

http://earth.geology.yale.edu/%7eajs/SupplementaryData/2020/Li

REFERENCES

Alexeiev, D. V., Biske, Y. S., Wang, B., Djenchuraeva, A. V., Getman, O. F., Aristov, V. A., Kröner, A., Liu, H., and Zhong, L., 2015, Tectono-Stratigraphic framework and Palaeozoic evolution of the Chinese South Tianshan: Geotectonics, v. 49, n. 2, p. 93–122, https://doi.org/10.1134/S0016852115020028

An, F., Zhu, Y., Wei, S., and Lai, S., 2017, The zircon U–Pb and Hf isotope constraints on the basement nature and Paleozoic evolution in northern margin of Yili Block, NW China: Gondwana Research, v. 43, p. 41–54, https://doi.org/10.1016/j.gr.2015.11.014

BGMRX, 1959, Geological map and explanatory note of the Kumishi sheet (Map K-45-XVII, scale 1:200,000): Xinjiang, China, Government Printer.

BGMRX, 1993, Bureau of Geology and Mineral Resources of Xinjiang Autonomous Region, Regional Geology of Xinjiang Autonomous Region (In Chinese with the English abstract): Beijing, China, Geological Publishing House, 841 p.

Biske, Y. S., Alexeiev, D. V., Ershova, V. B., Priyatkina, N. S., DuFrane, S. A., and Khudoley, A. K., 2019, Detrital zircon U-Pb geochronology of middle Paleozoic sandstones from the South Tianshan (Kyrgyzstan): Implications for provenance and tectonic evolution of the Turkestan Ocean: Gondwana Research, v. 75, p. 97–117, https://doi.org/10.1016/j.gr.2019.04.010

Briggs, S. M., Yin, A., Manning, C. E., Chen, Z.-L., Wang, X.-F., and Grove, M., 2007, Late Paleozoic tectonic history of the Ertix Fault in the Chinese Altai and its implications for the development of the Central Asian Orogenic System: GSA Bulletin, v. 119, n. 7–8, p. 944–960, https://doi.org/10.1130/B26044.1

Broussolle, A., Aguilar, C., Sun, M., Schulmann, K., Štípská, P., Jiang, Y., Yu, Y., Xiao, W., Wang, S., and Míková, J., 2018, Polycyclic Palaeozoic evolution of accretionary orogenic wedge in the southern Chinese Altai: Evidence from structural relationships and U-Pb geochronology: Lithos, v. 314–315, p. 400–424, https://doi.org/10.1016/j.lithos.2018.06.005

Buslov, M. M., Watanabe, T., Fujiwara, Y., Iwata, K., Smirnova, L. V., Safonova, I. Y., Semakov, N. N., and Kiryanova, A. P., 2004, Late Paleozoic faults of the Altai region, Central Asia: Tectonic pattern and model of formation: Journal of Asian Earth Sciences, v. 23, n. 5, p. 655–671, https://doi.org/10.1016/S1367-9120(03)00131-7

Cai, K., Sun, M., Yuan, C., Long, X., and Xiao, W., 2011, Geological framework and Paleozoic tectonic history of the Chinese Altai, NW China: A review: Russian Geology and Geophysics, v. 52, n. 12, p. 1619–1633, https://doi.org/10.1016/j.rgg.2011.11.014

Cai, K., Sun, M., Yuan, C., Xiao, W., Zhao, G., Long, X., and Wu, F., 2012a, Carboniferous mantle-derived felsic intrusion in the Chinese Altai, NW China: Implications for geodynamic change of the accretionary orogenic belt: Gondwana Research, v. 22, n. 2, p. 681–698, https://doi.org/10.1016/j.gr.2011.11.008

Cai, Z., Xu, Z., He, B., and Wang, R., 2012b, Age and tectonic evolution of ductile shear zones in the eastern Tianshan-Beishan orogenic belt: Acta Petrologica Sinica, v. 28, n. 6, p. 1875–1895 (In Chinese with the English abstract).

Charvet, J., Shu, L. S., and Laurent-Charvet, S., 2007, Paleozoic structural and geodynamic evolution of eastern Tianshan (NW China): Welding of the Tarim and Junggar plates: Episodes, v. 30, n. 3, p. 162–186.

Charvet, J., Shu, L., Laurent-Charvet, S., Wang, B., Faure, M., Cluzel, D., Chen, Y., and de Jong, K., 2011, Palaeozoic tectonic evolution of the Tianshan belt, NW China: Science China Earth Sciences, v. 54, n. 2, p. 166–184, https://doi.org/10.1007/s11430-010-4138-1

Chen, M., Sun, M., Li, P., Zheng, J., Cai, K., and Su, Y., 2019, Late Paleozoic Accretionary and Collisional Processes along the Southern Peri-Siberian Orogenic System: New Constraints from Amphibolites within the Irtysh Complex of Chinese Altai: The Journal of Geology, v. 127, n. 2, p. 241–262, https://doi.org/10.1086/701253

Cui, X., Sun, M., Zhao, G., Yao, J., Zhang, Y., Han, Y., and Dai, L., 2020, A Devonian arc–back-arc basin system in the southern Chinese Altai: Constraints from geochemical and Sr-Nd-Pb isotopic data for metabasaltic rocks: Lithos, v. 366–367, p. 105540, https://doi.org/10.1016/j.lithos.2020.105540

de Jong, K., Wang, B., Faure, M., Shu, L., Cluzel, D., Charvet, J., Ruffet, G., and Chen, Y., 2009, New $^{40}Ar/^{39}Ar$ age constraints on the Late Palaeozoic tectonic evolution of the western Tianshan (Xinjiang, northwestern China), with emphasis on Permian fluid ingress: International Journal of Earth Sciences, v. 98, n. 6, p. 1239–1258, https://doi.org/10.1007/s00531-008-0338-8

Deng, S. T., Guo, Z. J., Zhang, Z. C., and Liao, G. H., 2006, Timing of the formation of the Sangshuyuanzi ductile shear zone in the central segment of the South Tianshan and its tectonic significance: Geology in China, v. 81, n. 2, p. 641–647 (In Chinese with the English abstract).

Eizenhöfer, P. R., and Zhao, G., 2018, Solonker Suture in East Asia and its bearing on the final closure of the eastern segment of the Palaeo-Asian Ocean: Earth-Science Reviews, v. 186, p. 153–172, https://doi.org/10.1016/j.earscirev.2017.09.010

Filippova, I. B., Bush, V. A., and Didenko, A. N., 2001, Middle Paleozoic subduction belts: The leading factor in the formation of the Central Asian fold-and-thrust belt: Russian Journal of Earth Sciences, v. 3, n. 6, p. 405–426, https://doi.org/10.2205/2001ES000073

Frisch, W., Dunkl, I., and Kuhlemann, J., 2000, Post-collisional orogen-parallel large-scale extension in the Eastern Alps: Tectonophysics, v. 327, n. 3–4, p. 239–265, https://doi.org/10.1016/S0040-1951(00)00204-3

Gao, J., Li, M., Xiao, X., Tang, Y., and He, G., 1998, Paleozoic tectonic evolution of the Tianshan Orogen, northwestern China: Tectonophysics, v. 287, n. 3–4, p. 213–231, https://doi.org/10.1016/S0040-1951(98)80070-X

Gao, J., Long, L., Klemd, R., Qian, Q., Liu, D., Xiong, X., Su, W., Liu, W., Wang, Y., and Yang, F., 2009, Tectonic evolution of the South Tianshan orogen and adjacent regions, NW China: Geochemical and age constraints of granitoid rocks: International Journal of Earth Sciences, v. 98, n. 6, p. 1221–1238, https://doi.org/10.1007/s00531-008-0370-8

Glorie, S., De Grave, J., Delvaux, D., Buslov, M. M., Zhimulev, F. I., Vanhaecke, F., Elburg, M. A., and Van den haute, P., 2012, Tectonic history of the Irtysh shear zone (NE Kazakhstan): New constraints from zircon U/Pb dating, apatite fission track dating and palaeostress analysis: Journal of Asian Earth Sciences, v. 45, p. 138–149, https://doi.org/10.1016/j.jseaes.2011.09.024

Han, B. F., Guo, Z. J., Zhang, Z. C., Zhang, L., Chen, J. F., and Song, B., 2010, Age, geochemistry, and tectonic implications of a late Paleozoic stitching pluton in the North Tian Shan suture zone, western China: GSA Bulletin, v. 122, n. 3–4, p. 627–640, https://doi.org/10.1130/B26491.1

Han, B. F., He, G. Q., Wang, X. C., and Guo, Z. J., 2011, Late Carboniferous collision between the Tarim and Kazakhstan–Yili terranes in the western segment of the South Tian Shan Orogen, Central Asia, and implications for the Northern Xinjiang, western China: Earth-Science Reviews, v. 109, n. 3–4, p. 74–93, https://doi.org/10.1016/j.earscirev.2011.09.001

Han, Y., and Zhao, G., 2018, Final amalgamation of the Tianshan and Junggar orogenic collage in the southwestern Central Asian Orogenic Belt: Constraints on the closure of the Paleo-Asian Ocean: Earth-Science Reviews, v. 186, p. 129–152, https://doi.org/10.1016/j.earscirev.2017.09.012

He, J., Zhu, W., Zheng, B., Wu, H., Cui, X., and Lu, Y., 2015, Neoproterozoic diamictite-bearing sedimentary rocks in the northern Yili Block and their constraints on the Precambrian evolution of microcontinents in the Western Central Asian Orogenic Belt: Tectonophysics, v. 665, p. 23–36, https://doi.org/10.1016/j.tecto.2015.09.021

Hu, W., Li, P., Rosenbaum, G., Liu, J., Jourdan, F., Jiang, Y., Wu, D., Zhang, J., Yuan, C., and Sun, M., 2020, Structural evolution of the eastern segment of the Irtysh Shear Zone: Implications for the collision between the East Junggar Terrane and the Chinese Altai Orogen (northwestern China): Journal of Structural Geology, v. 139, https://doi.org/10.1016/j.jsg.2020.104126

Huang, Z., Long, X., Kröner, A., Yuan, C., Wang, Y., Chen, B., and Zhang, Y., 2015, Neoproterozoic granitic gneisses in the Chinese Central Tianshan Block: Implications for tectonic affinity and Precambrian crustal evolution: Precambrian Research, v. 269, p. 73–89, https://doi.org/10.1016/j.precamres.2015.08.005

Huang, Z., Long, X., Yuan, C., Sun, M., Wang, Y., Zhang, Y., and Chen, B., 2016, Detrital zircons from Neoproterozoic sedimentary rocks in the Yili Block: Constraints on the affinity of microcontinents in the southern Central Asian Orogenic Belt: Gondwana Research, v. 37, p. 39–52, https://doi.org/10.1016/j.gr.2016.05.009

Janots, E., Engi, M., Berger, A., Allaz, J., Schwarz, J. O., and Spandler, C., 2008, Prograde metamorphic sequence of REE minerals in pelitic rocks of the Central Alps: Implications for allanite–monazite–xenotime phase relations from 250 to 610°C: Journal of Metamorphic Geology, v. 26, n. 5, p. 509–526, https://doi.org/10.1111/j.1525-1314.2008.00774.x

Jiang, T., Gao, J., Klemd, R., Qian, Q., Zhang, X., Xiong, X., Wang, X., Tan, Z., and Chen, B., 2014, Paleozoic ophiolitic mélanges from the South Tianshan Orogen, NW China: Geological, geochemical and geochronological implications for the geodynamic setting: Tectonophysics, v. 612–613, p. 106–127, https://doi.org/10.1016/j.tecto.2013.11.038

Jiang, Y. D., Schulmann, K., Sun, M., Weinberg, R. F., Štípská, P., Li, P. F., Zhang, J., Chopin, F., Wang, S., Xia, X. P., and Xiao, W. J., 2019, Structural and geochronological constraints on Devonian suprasubduction tectonic switching and Permian collisional dynamics in the Chinese Altai, Central Asia: Tectonics, v. 38, n. 1, p. 253–280, https://doi.org/10.1029/2018TC005231

Konopelko, D., Seltmann, R., Apayarov, F., Belousova, E., Izokh, A., and Lepekhina, E., 2013, U–Pb–Hf zircon study of two mylonitic granite complexes in the Talas-Fergana fault zone, Kyrgyzstan, and Ar–Ar age of deformations along the fault: Journal of Asian Earth Sciences, v. 73, p. 334–346, https://doi.org/10.1016/j.jseaes.2013.04.046

Konopelko, D., Klemd, R., Petrov, S. V., Apayarov, F., Nazaraliev, B., Vokueva, O., Scherstén, A., and Sergeev, S., 2017, Precambrian gold mineralization at Djamgyr in the Kyrgyz Tien Shan: Tectonic and metallogenic implications: Ore Geology Reviews, v. 86, p. 537–547, https://doi.org/10.1016/j.oregeorev.2017.03.007

Laurent-Charvet, S., Charvet, J., Shu, L., Ma, R., and Lu, H., 2002, Palaeozoic late collisional strike-slip deformations in Tianshan and Altay, Eastern Xinjiang, NW China: Terra Nova, v. 14, n. 4, p. 249–256, https://doi.org/10.1046/j.1365-3121.2002.00417.x

Laurent-Charvet, S., Charvet, J., Monié, P., and Shu, L., 2003, Late Paleozoic strike-slip shear zones in eastern Central Asia (NW China): New structural and geochronological data: Tectonics, v. 22, n. 2, https://doi.org/10.1029/2001TC901047

Li, P., Sun, M., Rosenbaum, G., Cai, K., and Yu, Y., 2015a, Structural evolution of the Irtysh Shear Zone (northwestern China) and implications for the amalgamation of arc systems in the Central Asian Orogenic Belt: Journal of Structural Geology, v. 80, p. 142–156, https://doi.org/10.1016/j.jsg.2015.08.008

Li, P., Yuan, C., Sun, M., Long, X., and Cai, K., 2015b, Thermochronological constraints on the late Paleozoic tectonic evolution of the southern Chinese Altai: Journal of Asian Earth Sciences, v. 113, Part 1, p. 51–60, https://doi.org/10.1016/j.jseaes.2014.11.004

Li, P., Sun, M., Rosenbaum, G., Cai, K., Chen, M., and He, Y., 2016, Transpressional deformation, strain partitioning and fold superimposition in the southern Chinese Altai, Central Asian Orogenic Belt: Journal of Structural Geology, v. 87, p. 64–80, https://doi.org/10.1016/j.jsg.2016.04.006

Li, P., Sun, M., Rosenbaum, G., Jourdan, F., Li, S., and Cai, K., 2017, Late Paleozoic closure of the Ob-Zaisan Ocean along the Irtysh shear zone (NW China): Implications for arc amalgamation and oroclinal bending in the Central Asian orogenic belt: GSA Bulletin, v. 129, n. 5–6, p. 547–569, https://doi.org/10.1130/B31541.1

Li, P., Sun, M., Rosenbaum, G., Yuan, C., Safonova, I., Cai, K., Jiang, Y., and Zhang, Y., 2018, Geometry, kinematics and tectonic models of the Kazakhstan Orocline, Central Asian Orogenic Belt: Journal of Asian Earth Sciences, v. 153, p. 42–56, https://doi.org/10.1016/j.jseaes.2017.07.029

Li, P., Sun, M., Shu, C., Yuan, C., Jiang, Y., Zhang, L., and Cai, K., 2019, Evolution of the Central Asian Orogenic Belt along the Siberian margin from Neoproterozoic-Early Paleozoic accretion to Devonian trench retreat and a comparison with Phanerozoic eastern Australia: Earth-Science Reviews, v. 198, p. 102951, https://doi.org/10.1016/j.earscirev.2019.102951

Li, P., Sun, M., Rosenbaum, G., Cai, K., Yuan, C., Jourdan, F., Xia, X., Jiang, Y., and Zhang, Y., 2020, Tectonic evolution of the Chinese Tianshan Orogen from subduction to arc-continent collision: Insight from polyphase deformation along the Gangou section, Central Asia: GSA Bulletin, v. 132, n. 11–12, p. 2529–2552, https://doi.org/10.1130/B35353.1

Li, Q., and Zhang, L., 2004, The P-T path and geological significance of low-pressure granulite-facies metamorphism in Muzhaerte, southwest Tianshan: Acta Petrologica Sinica, v. 20, n. 3, p. 583–594 (In Chinese with the English abstract).

Li, Q., Liu, S., Wang, Z., Han, B., Shu, G., and Wang, T., 2008, Electron microprobe monazite geochronological constraints on the Late Palaeozoic tectonothermal evolution in the Chinese Tianshan: Journal of the Geological Society, London, v. 165, n. 2, p. 511–522, https://doi.org/10.1144/0016-76492007-077

Li, Z., Yang, X., Li, Y., Santosh, M., Chen, H., and Xiao, W., 2014, Late Paleozoic tectono–metamorphic evolution of the Altai segment of the Central Asian Orogenic Belt: Constraints from metamorphic P–T pseudosection and zircon U–Pb dating of ultra-high-temperature granulite: Lithos, v. 204, p. 83–96, https://doi.org/10.1016/j.lithos.2014.05.022

Lin, W., Faure, M., Shi, Y., Wang, Q., and Li, Z., 2009, Palaeozoic tectonics of the south-western Chinese Tianshan: New insights from a structural study of the high-pressure/low-temperature metamorphic belt: International Journal of Earth Sciences, v. 98, n. 6, p. 1259–1274, https://doi.org/10.1007/s00531-008-0371-7

Liu, F., Wang, Z., Lin, W., Chen, K., Jiang, L., and Wang, Q., 2013, Structure deformation and tectonic significance of Erqis fault zone in the southern margin of Chinese Altay: Acta Petrologica Sinica, v. 29, n. 5, p. 1811–1824 (In Chinese with the English abstract).

Liu, Z., Bartoli, O., Tong, L., Xu, Y. G., and Huang, X., 2020, Permian ultrahigh–temperature reworking in the southern Chinese Altai: Evidence from petrology, P–T estimates, zircon and monazite U–Th–Pb geochronology: Gondwana Research, v. 78, p. 20–40, https://doi.org/10.1016/j.gr.2019.08.007

Long, X., Yuan, C., Sun, M., Xiao, W., Wang, Y., Cai, K., and Jiang, Y., 2012, Geochemistry and Nd isotopic composition of the Early Paleozoic flysch sequence in the Chinese Altai, Central Asia: Evidence for a northward-derived mafic source and insight into Nd model ages in accretionary orogen: Gondwana Research, v. 22, n. 2, p. 554–566, https://doi.org/10.1016/j.gr.2011.04.009

Norris, R. J., and Toy, V. G., 2014, Continental transforms: A view from the Alpine Fault: Journal of Structural Geology, v. 64, p. 3–31, https://doi.org/10.1016/j.jsg.2014.03.003

Qu, G., and Zhang, J., 1994, Oblique thrust systems in the Altay orogen, China: Journal of Southeast Asian Earth Sciences, v. 9, n. 3, p. 277–287, https://doi.org/10.1016/0743-9547(94)90035-3

Rolland, Y., Alexeiev, D. V., Kröner, A., Corsini, M., Loury, C., and Monié, P., 2013, Late Palaeozoic to Mesozoic kinematic history of the Talas–Ferghana strike-slip fault (Kyrgyz West Tianshan) as revealed by $^{40}Ar/^{39}Ar$ dating of syn-kinematic white mica: Journal of Asian Earth Sciences, v. 67–68, p. 76–92, https://doi.org/10.1016/j.jseaes.2013.02.012

Selverstone, J., 2005, Are the Alps collapsing?: Annual Review of Earth and Planetary Sciences, v. 33, n. 1, p. 113–132, https://doi.org/10.1146/annurev.earth.33.092203.122535

Şengör, A. M. C., and Natal'in, B. A., 1996, Turkic-type orogeny and its role in the making of the continental crust: Annual Review of Earth and Planetary Sciences, v. 24, n. 1, p. 263–337, https://doi.org/10.1146/annurev.earth.24.1.263

Şengör, A. M. C., Natal'in, B. A., and Burtman, V. S., 1993, Evolution of the Altaid tectonic collage and Palaeozoic crustal growth in Eurasia: Nature, v. 364, n. 6435, p. 299–307, https://doi.org/10.1038/364299a0

Şengör, A. M. C., Natal'in, B., Sunal, G., and van der Voo, R., 2018, The tectonics of the Altaids: Crustal growth during the construction of the continental lithosphere of Central Asia between ~750 and ~130 Ma ago: Annual Review of Earth and Planetary Sciences, v. 46, n. 1, p. 439–494, https://doi.org/10.1146/annurev-earth-060313-054826

Shi, Y., Liu, D., Zhang, Q., Jian, P., Zhang, F., and Miao, L., 2007, SHRIMP zircon U-Pb dating of the Gangou granitoids, Central Tianshan Mountains, Northwest China and tectonic significances: Chinese Science Bulletin, v. 52, n. 11, p. 1507–1516, https://doi.org/10.1007/s11434-007-0204-2

Shu, L., Charvet, J., Guo, L., Lu, H., and Laurent-Charvet, S., 1999, A large-scale Palaeozoic dextral ductile strike-slip zone: The Aqqikkudug-Weiya zone along the northern margin of the central Tianshan Belt, Xinjiang, NW China: Acta Geologica Sinica, v. 73, n. 2, p. 148–162, https://doi.org/10.1111/j.1755-6724.1999.tb00822.x

Tang, G. J., Chung, S. L., Hawkesworth, C. J., Cawood, P. A., Wang, Q., Wyman, D. A., Xu, Y. G., and Zhao, Z. H., 2017, Short episodes of crust generation during protracted accretionary processes: Evidence from Central Asian Orogenic Belt, NW China: Earth and Planetary Science Letters, v. 464, p. 142–154, https://doi.org/10.1016/j.epsl.2017.02.022

Tapponnier, P., Peltzer, G., Le Dain, A. Y., Armijo, R., and Cobbold, P., 1982, Propagating extrusion tectonics in Asia: New insights from simple experiments with plasticine: Geology, v. 10, n. 12, p. 611–616, https://doi.org/10.1130/0091-7613(1982)10<611:PETIAN>2.0.CO;2

Tong, Y., Wang, T., Jahn, B. M., Sun, M., Hong, D. W., and Gao, J. F., 2014, Post-accretionary permian granitoids in the Chinese Altai orogen: Geochronology, petrogenesis and tectonic implications: American Journal of Science, v. 314, n. 1, p. 80–109, https://doi.org/10.2475/01.2014.03

Wang, B., Faure, M., Cluzel, D., Shu, L., Charvet, J., Meffre, S., and Ma, Q., 2006, Late Paleozoic tectonic evolution of the northern West Chinese Tianshan Belt: Geodinamica Acta, v. 19, n. 3–4, p. 237–247, https://doi.org/10.3166/ga.19.237-247

Wang, B., Shu, L. S., Cluzel, D., Faure, M., and Charvet, J., 2007a, Geochemical constraints on Carboniferous volcanic rocks of the Yili Block (Xinjiang, NW China): Implication for the tectonic evolution of Western Tianshan: Journal of Asian Earth Sciences, v. 29, n. 1, p. 148–159, https://doi.org/10.1016/j.jseaes.2006.02.008

Wang, B., Shu, L. S., Faure, M., Cluzel, D., and Charvet, J., 2007b, Paleozoic tectonism and magmatism of Kekesu-Qiongkushitai section in southwestern Chinese Tianshan and their constraints on the age of the orogeny: Acta Petrologica Sinica, v. 23, n. 6, p. 1354–1368.

Wang, B., Cluzel, D., Shu, L., Faure, M., Charvet, J., Chen, Y., Meffre, S., and de Jong, K., 2009, Evolution of calc-alkaline to alkaline magmatism through Carboniferous convergence to Permian transcurrent tectonics, western Chinese Tianshan: International Journal of Earth Sciences, v. 98, n. 6, p. 1275–1298, https://doi.org/10.1007/s00531-008-0408-y

Wang, B., Faure, M., Shu, L., de Jong, K., Charvet, J., Cluzel, D., Jahn, B-m., Chen, Y., and Ruffet, G., 2010a, Structural and geochronological study of high-pressure metamorphic rocks in the Kekesu section (northwestern China): Implications for the late Paleozoic tectonics of the Southern Tianshan: The Journal of Geology, v. 118, n. 1, p. 59–77, https://doi.org/10.1086/648531

Wang, B., Jahn, B., Lo, C., Shu, L., Wu, C., Li, K., and Wang, F., 2011a, Structural analysis and $^{40}Ar/^{39}Ar$ thermochronology of Proterozoic rocks in Sailimu area (NW China): Implication to polyphase tectonics of the North Chinese Tianshan: Journal of Asian Earth Sciences, v. 42, n. 5, p. 839–853, https://doi.org/10.1016/j.jseaes.2011.07.022

Wang, B., Shu, L., Faure, M., Jahn, B., Cluzel, D., Charvet, J., Chung, S., and Meffre, S., 2011b, Paleozoic tectonics of the southern Chinese Tianshan: Insights from structural, chronological and geochemical studies of the Heiyingshan ophiolitic mélange (NW China): Tectonophysics, v. 497, n. 1-4, p. 85–104, https://doi.org/10.1016/j.tecto.2010.11.004

Wang, B., Cluzel, D., Jahn, B.-m., Shu, L., Chen, Y., Zhai, Y., Branquet, Y., Barbanson, L., and Sizaret, S., 2014a, Late Paleozoic pre-and syn-kinematic plutons of the Kangguer–Huangshan Shear zone: Inference on the tectonic evolution of the eastern Chinese north Tianshan: American Journal of Science, v. 314, n. 1, p. 43–79, https://doi.org/10.2475/01.2014.02

Wang, B., Zhai, Y., Kapp, P., de Jong, K., Zhong, L., Liu, H., Ma, Y., Gong, H., and Geng, H., 2018, Accretionary tectonics of back-arc oceanic basins in the South Tianshan: Insights from structural, geochronological, and geochemical studies of the Wuwamen ophiolite mélange: GSA Bulletin, v. 130, n. 1–2, p. 581–582, https://doi.org/10.1130/B31397.1

Wang, H., 2007, Geological Map of Chinese Tianshan and Adjacent Areas: Xi'an, China, Xi'an Center of Geological Survey, Chinese Geological Survey, scale 1: 1,000,000.

Wang, Q. C., Shu, L. S., Charvet, J., Faure, M., Ma, H. D., Natal'in, B., Gao, J., Kroner, A., Xiao, W. J., Li, J. Y., Windley, B., Chen, Y., Glen, R., Jian, P., Zhang, W., Seltmann, R., Wilde, S., Choulet, F., Wan, B., Quinn, C., Rojas-Agramonte, Y., Shang, Q. H., Zhang, W., Wang, B., and Lin, W., 2010b, Understanding and study perspectives on tectonic evolution and crustal structure of the Paleozoic Chinese Tianshan: Episodes, v. 33, n. 4, p. 242–266, https://doi.org/10.18814/epiiugs/2010/v33i4/003

Wang, W., Wei, C., Zhang, Y., Chu, H., Zhao, Y., and Liu, X., 2014b, Age and origin of sillimanite schist from the Chinese Altai metamorphic belt: Implications for late Palaeozoic tectonic evolution of the Central Asian Orogenic Belt: International Geology Review, v. 56, n. 2, p. 224–236, https://doi.org/10.1080/00206814.2013.841335

Wang, Y., Li, J., and Sun, G., 2008, Postcollisional Eastward Extrusion and Tectonic Exhumation along the Eastern Tianshan Orogen, Central Asia: Constraints from Dextral Strike-Slip Motion and $^{40}Ar/^{39}Ar$ Geochronological Evidence: The Journal of Geology, v. 116, n. 6, p. 599–618, https://doi.org/10.1086/591993

Wilhem, C., Windley, B. F., and Stampfli, G. M., 2012, The Altaids of Central Asia: A tectonic and evolutionary innovative review: Earth-Science Reviews, v. 113, n. 3–4, p. 303–341, https://doi.org/10.1016/j.earscirev.2012.04.001

Windley, B. F., Kröner, A., Guo, J., Qu, G., Li, Y., and Zhang, C., 2002, Neoproterozoic to Paleozoic geology of the Altai Orogen, NW China: New zircon age data and tectonic evolution: The Journal of Geology, v. 110, n. 6, p. 719–737, https://doi.org/10.1086/342866

Windley, B. F., Alexeiev, D., Xiao, W., Kroner, A., and Badarch, G., 2007, Tectonic models for accretion of the Central Asian Orogenic Belt: Journal of the Geological Society, v. 164, n. 1, p. 31–47, https://doi.org/10.1144/0016-76492006-022

Xiao, W., and Santosh, M., 2014, The western Central Asian Orogenic Belt: A window to accretionary orogenesis and continental growth: Gondwana Research, v. 25, n. 4, p. 1429–1444, https://doi.org/10.1016/j.gr.2014.01.008

Xiao, W., Zhang, L., Qin, K., Sun, S., and Li, J., 2004, Paleozoic accretionary and collisional tectonics of the Eastern Tianshan (China): Implications for the continental growth of central Asia: American Journal of Science, v. 304, n. 4, p. 370–395, https://doi.org/10.2475/ajs.304.4.370

Xiao, W., Windley, B. F., Huang, B. C., Han, C. M., Yuan, C., Chen, H. L., Sun, M., Sun, S., and Li, J. L., 2009a, End-Permian to mid-Triassic termination of the accretionary processes of the southern Altaids: Implications for the geodynamic evolution, Phanerozoic continental growth, and metallogeny of Central Asia: International Journal of Earth Sciences, v. 98, n. 6, p. 1189–1217, https://doi.org/10.1007/s00531-008-0407-z

Xiao, W. J., Windley, B. F., Yuan, C., Sun, M., Han, C. M., Lin, S. F., Chen, H. L., Yan, Q. R., Liu, D. Y., Qin, K. Z., Li, J. L., and Sun, S., 2009b, Paleozoic multiple subduction-accretion processes of the southern Altaids: American Journal of Science, v. 309, n. 3, p. 221–270, https://doi.org/10.2475/03.2009.02

Xiao, W., Han, C., Yuan, C., Sun, M., Zhao, G., and Shan, Y., 2010a, Transitions among Mariana-, Japan-, Cordillera-and Alaska-type arc systems and their final juxtapositions leading to accretionary and collisional orogenesis: Geological Society, London, Special Publications, v. 338, n. 1, p. 35–53, https://doi.org/10.1144/SP338.3

Xiao, W., Huang, B., Han, C., Sun, S., and Li, J., 2010b, A review of the western part of the Altaids: A key to understanding the architecture of accretionary orogens: Gondwana Research, v. 18, n. 2–3, p. 253–273, https://doi.org/10.1016/j.gr.2010.01.007

Xiao, W., Windley, B. F., Allen, M. B., and Han, C., 2013, Paleozoic multiple accretionary and collisional tectonics of the Chinese Tianshan orogenic collage: Gondwana Research, v. 23, n. 4, p. 1316–1341, https://doi.org/10.1016/j.gr.2012.01.012

Xiao, W., Windley, B. F., Sun, S., Li, J., Huang, B., Han, C., Yuan, C., Sun, M., and Chen, H., 2015, A Tale of amalgamation of three Permo-Triassic Collage Systems in Central-East Asia: Oroclines, sutures, and Terminal Accretion: Annual Review of Earth and Planetary Sciences, v. 43, n. 1, p. 477–507, https://doi.org/10.1146/annurev-earth-060614-105254

Xu, Z., Wang, Q., Pêcher, A., Liang, F., Qi, X., Cai, Z., Li, H., Zeng, L., and Cao, H., 2013, Orogen-parallel ductile extension and extrusion of the Greater Himalaya in the late Oligocene and Miocene: Tectonics, v. 32, n. 2, p. 191–215, https://doi.org/10.1002/tect.20021

Yang, T. N., Wang, Y., Li, J. Y., and Sun, G. H., 2007, Vertical and horizontal strain partitioning of the Central Tianshan (NW China): Evidence from structures and $^{40}Ar/^{39}Ar$ geochronology: Journal of Structural Geology, v. 29, n. 10, p. 1605–1621, https://doi.org/10.1016/j.jsg.2007.08.002

Yang, T. N., Li, J. Y., Wang, Y., and Dang, Y. X., 2009, Late Early Permian (266 Ma) N–S compressional deformation of the Turfan basin, NW China: The cause of the change in basin pattern: International Journal of Earth Sciences, v. 98, n. 6, p. 1311–1324, https://doi.org/10.1007/s00531-008-0396-y

Yin, A., and Nie, S., 1996, A Phanerozoic Palinspastic Reconstruction of China and its Neighboring Regions, *in* Yian, A., and Harrison, T. A., editors, The tectonic evolution of Asia: New York; Cambridge University Press, p. 442–485.

Zhang, C., Liu, D., Luo, Q., Liu, L., Zhang, Y., Zhu, D., Wang, P., and Dai, Q., 2018, An evolving tectonic environment of Late Carboniferous to Early Permian granitic plutons in the Chinese Altai and Eastern Junggar terranes, Central Asian Orogenic Belt, NW China: Journal of Asian Earth Sciences, v. 159, p. 185–208, https://doi.org/10.1016/j.jseaes.2017.08.008

Zhang, C. L., Santosh, M., Zou, H. B., Xu, Y. G., Zhou, G., Dong, Y. G., Ding, R. F., and Wang, H. Y., 2012, Revisiting the "Irtish tectonic belt": Implications for the Paleozoic tectonic evolution of the Altai orogen: Journal of Asian Earth Sciences, v. 52, p. 117–133, https://doi.org/10.1016/j.jseaes.2012.02.016

Zhang, X., Zhao, G., Sun, M., Eizenhöfer, P. R., Han, Y., Hou, W., Liu, D., Wang, B., Liu, Q., and Xu, B., 2016, Tectonic evolution from subduction to arc-continent collision of the Junggar ocean: Constraints from U-Pb dating and Hf isotopes of detrital zircons from the North Tianshan belt, NW China: GSA Bulletin, v. 128, n. 3–4, p. 644–660, https://doi.org/10.1130/B31230.1

Zhang, Y., Yuan, C., Sun, M., Long, X., Huang, Z., Jiang, Y., Li, P., and Du, L., 2020, Two late Carboniferous belts of Nb-enriched mafic magmatism in the Eastern Tianshan: Heterogeneous mantle sources and geodynamic implications: GSA Bulletin, v. 132, n. 9–10, p. 1863–1880, https://doi.org/10.1130/B35366.1

Zhao, G., Wang, Y., Huang, B., Dong, Y., Li, S., Zhang, G., and Yu, S., 2018, Geological reconstructions of the East Asian blocks: From the breakup of Rodinia to the assembly of Pangea: Earth-Science Reviews, v. 186, p. 262–286, https://doi.org/10.1016/j.earscirev.2018.10.003

Zhong, L., Wang, B., de Jong, K., Zhai, Y., and Liu, H., 2019, Deformed continental arc sequences in the South Tianshan: New constraints on the Early Paleozoic accretionary tectonics of the Central Asian Orogenic Belt: Tectonophysics, v. 768, 228169, https://doi.org/10.1016/j.tecto.2019.228169

Zhou, D., Graham, S. A., Chang, E. Z., Wang, B., and Hacker, B., 2001, Paleozoic tectonic amalgamation of the Chinese Tian Shan: Evidence from a transect along the Dushanzi-Kuqa Highway, *in* Hendrix, M. S., and Davis, G. A., editors, Paleozoic and Mesozoic tectonic evolution of central Asia: From continental assembly to intracontinental deformation: Geological Society of America Memoirs, v. 194, p. 23–46, https://doi.org/10.1130/0-8137-1194-0.23

Zhu, X., Wang, B., Chen, Y., Liu, H., Horng, C. s., Choulet, F., Faure, M., Shu, L., and Xue, Z., 2018, First Early Permian paleomagnetic pole for the Yili Block and its implications for Late Paleozoic post-orogenic kinematic evolution of the SW Central Asian Orogenic Belt: Tectonics, v. 37, n. 6, p. 1709–1732, https://doi.org/10.1029/2017TC004642